ISTANBUL TECHNICAL UNIVERSITY ★ GRADUATE SCHOOL OF SCIENCE ENGINEERING AND TECHNOLOGY

A NOVEL SPRING-LIKE CELLULAR STRUCTURE DESIGN FOR ENERGY ABSORBING APPLICATIONS

M.Sc. THESIS

Aren BOYACI

Department of Mechanical Engineering

Solid Mechanics Programme

JUNE 2017

ISTANBUL TECHNICAL UNIVERSITY ★ GRADUATE SCHOOL OF SCIENCE ENGINEERING AND TECHNOLOGY

A NOVEL SPRING-LIKE CELLULAR STRUCTURE DESIGN FOR ENERGY ABSORBING APPLICATIONS

M.Sc. THESIS

Aren BOYACI

Department of Mechanical Engineering

Solid Mechanics Programme

Thesis Advisor: Asst. Prof. Dr. Mesut KIRCA

JUNE 2017

ISTANBUL TEKNİK ÜNİVERSİTESİ ★ FEN BİLİMLERİ ENSTİTÜSÜ

ENERJİ EMİCİ UYGULAMALAR İÇİN YAY-BENZERİ HÜCRE YAPI TASARIMI

YÜKSEK LİSANS TEZİ

Aren BOYACI
503151502

Makina Mühendisliği Anabilim Dalı

Katı Cisimlerin Mekaniği Programı

Tez Danışmanı: Yrd. Doç. Dr. Mesut KIRCA

HAZİRAN 2017

Aren Boyacı, a M.Sc. student of ITU Graduate School of Science Engineering and Technology student **ID 503151502**, successfully defended the **thesis** entitled "**A Novel Spring-Like Cellular Structure Design for Energy Absorbing Applications**", which he prepared after fulfilling the requirements specified in the associated legislations, before the jury whose signatures are below.

Thesis Advisor :	**Asst. Prof. Dr. Mesut KIRCA** Istanbul Technical University	.....
Jury Members :	**Assoc. Prof. Dr. M. Salih Dokuz** Istanbul Technical University	.....
	Asst. Prof. Dr. Emrecan Söylemez Marmara University	.....

Date of Submission : 5 May 2017
Date of Defense : 8 June 2017

To my family,

FOREWORD

I present my sincerest thanks to the people, my supervisor, family and friends, who have helped me, supported me, and encouraged me along the journey of my Master. I am so grateful to have those people among my side for their kindness, and knowing that they are there to help me gave me strength along this journey.

Firstly, I would like to thank my thesis supervisor Asst. Prof. Dr. Mesut Kirca for his kindness, guidance, and helping to solve the problems I came across. I would not be able to finish this thesis without his support.

Secondly, and most importantly I would like to present my sincerest thanks to my family. Knowing them supporting me no matter I fail or not gave me strength and encoureged me. It is not possible to express what it means for me with words.

June 2017

Aren Boyacı
(Mechanical Engineer)

TABLE OF CONTENTS

Page

ABBREVIATIONS

AM	**:** Additive Manufacturing
FEM	**:** Finite Element Method
FEA	**:** Finite Element Analysis
ABS	**:** Acrylonitrile-Butadiene-Styrene
CAD	**:** Computer-Aided Design
SEA	**:** Specific Energy Absorption
CFRP	**:** Carbon Fiber Reinforced Plastic
UV	**:** Ultraviolet
SLS	**:** Selective Laser Sintering
PBF	**:** Powder Bed Fusion
DMLS	**:** Direct Metal Laser Sintering

LIST OF TABLES

Page

TABLE OF FIGURES

Page

A NOVEL SPRING-LIKE CELLULAR STRUCTURE DESIGN FOR ENERGY ABSORBING APPLICATIONS

SUMMARY

With the outstanding development of additive manufacturing (AM) process, highly complex geometries became producible. Now it is possible to design a complex structure by using computer aided drawing (CAD) softwares, analyze it with finite element method (FEM) to see if it works well and lastly produce it with AM technology. AM plays a vital role to bring these designs to life.

In this thesis, a complex geometry is generated as CAD data, analyzed with finite element analysis (FEA) and redesigned until the most effective design is found, and the results are presented. The aim is to design a novel spring-like cellular structure to have high energy absorption capacity. The structure designed in this thesis is specialized as an energy absorbant structure under static and dynamic loads.

At the very beginning, additive manufacturing is briefly explained, cellular structures are defined and the literature is scanned to see the previously designed additevely manufactured, complex, light-weighted, and energy absorpant structures. The common qualities of the best designs are noted, and the aspects of the poorly designed structures are investigated to design a better structure. After the structure is designed, its parameters are defined and the effects of the parameters are investigated. By doing this, the optimum structure is tried to determined. Later on, when the design and modification processes are over, the model is tested under dynamic loading with help of FEA and results are presented. To do this, the design is simplified since the analysis of the structure takes very long time. The structure is simplified with analytical springs, and two different methods are used for this simplfication process. At the end, when those analyses are made, the energy absorption characteristics of both the actual 3D model and simplified models are calculated and compared. Those results are presented in the results chapter, and compared in the conclusion chapter.

ENERJİ EMİCİ UYGULAMALAR İÇİN YAY-BENZERİ HÜCRE YAPI TASARIMI

ÖZET

Katmanlı üretim teknolojisinin gelişmesiyle beraber, karmaşık geometrilere sahip yapılar üretilebilir hale geldi. Bu yapılar klasik parça eksiltme yöntemleriyle üretilmesi neredeyse imkansız veya çok maliyetli yapılardı. Katmanlı üretim teknolojisi sayesinde, bu karmaşık yapılar üretilebilir hale gelmekten öte daha da önem kazandı. Ve artık bu teknoloji sayesinde günümüzde bu yapılar CAD programlarında dizayn edilip, bir parça ekleme yöntemi olan katmanlı ğretim teknolojisiyle çok kolay bir şekilde üretilebiliyorlar. Katmanlı üretim teknolojisi, isminden de anlaşılacağı gibi parçaları katman katman üst üste ekleyip CAD verisi üzerinden üretim yapmaktadır. Bu sayede CAD programlarında atsarlanmış bu yapılar, gerektiği takdirde sonlu elemanlar yöntemiyle analiz edildikten sonra optimum hale getirilip gerçek hayattaki uygulamalarda kullanılabiliyor. Bu süreçte, katmanlı üretim teknolojisinin rolü oldukça önemli, çünkü bu dizaynlar, analizler ve modeldeki iyileştirmelerin bir üretim yöntemi eksikliğinde hiçbir önemi kalmazdı. Bu yöntem yapılan tasarımların dijital bir veriden öteye geçip, gerçek hayattaki uygulama alanlarında kullanılmasına ön ayak olmuştur.

Bu tezde, karmaşık bir yapıya sahip bir hücre yapı tasarlanmış, statik analizleri yapılıp iyileştirilmiş ve dinamik analizler sonucunda enerji emme kapasitesi sonuçları sunulmuştur. Bu tezin amacı, enerji emme kapasitesi yüksek yeni bir yay-benzeri hücre yapı tasarlamaktır. Bahsedilen bu yay-benzeri hücre yapı, statik ve dinamik yükler altında yüksek enerji emici kapasiteli bir yapı olarak tasarlanmıştır.

Tezin giriş kısmında, katmanlı üretim teknolojileri hakkında bilgi verilmiş ve yaygın yöntemlerinden bazılarından kısaca bahsedilmiştir.

Ayrıca bu tezdeki amaçla amaçları örtüşen literatürdeki benzer hücre yapılardan bahsedilmiş, örnekler verilmiş ve literatürdeki bu örneklerin ortak noktaları

belirtilmiştir. Bu yapılar tasarlanırken nelere dikkat edildiği, nasıl bir yol izlendiği not edilmiş ve bunlar bu tezde de uygulanmaya çalışılmıştır. Literatürdeki bu çalışmaların ortak iyi noktaları, ve ortak zayıf noktaları incelenmiş ve tasarlanan yeni model bu doğrultuda olmuştur.

Literatürde bir benzeri olmayan bir model tasarlanmış, önceki çalışmalarda yapılan hatalardan kaçınılmış ve az önce de bahsedilen ortak güçlü noktalar bu modelde harmanlanmaya çalışılmıştır. Model tasarlandıktan sonra parametreleri belirlenmiş, ve bu parameterlerin modele olan etkileri statik sonlu elemanlar yöntemleriyle incelenmiştir. Bu analizler ışığında optimum olduğu düşünülen paremetrelerle dizayn iyileştirilmiş, ve en iyi üç model belirlenmiştir. Bu tezde bu optimum olduğu düşünülen üç model dinamik sonlu elemanlar analizleri ile test edilmiştir. Ancak tasarlanan üç boyutlu modelin, ince ayrıntılara sahip olması ve tezde daha detaylıca bahsedilen sebeplerden dolayı analiz çok uzun sürmüştür. Bu sebeple modeli basitleştirmek için, hücre yapılar analitik yaylara indirgenip analizler bu şekilde yapılmaya çalışılmıştır.

Model, basitleştirirken iki yöntem kullanılmıştır. Bu yöntemlerden birinde 8 tane hücre yapıdan meydana gelmiş sandviç yapının hepsi tek bir yaya indirgenirken, ikinci yöntemde her hücre yapı için bir yay kullanılmıştır. Bu iki modelin de verdiği sonuçlar birbirlerine çok benzer olmakla beraber, dinamik analizi yapılan 3 boyutlu asıl modelde yakınsayabildikleri noktalar değişiklik göstermektedir. Bu karşılaştırmalar ve benzerlikler, tüm analizlerin sonuçları ve yorumları tezin sonuç kısmında ve tartışma kısmında sunulmuştur.

Yapılan karşılaştırmalar sonucunda, basitleştirilmiş analizlerin asıl üç boyutlu modelin analizinde ulaşılan bazı sonuçları verebildiği görülmüştür. Basitleştirilme yapılmayan analiz yaklaşık 9 gün sürerken, basitleştirilmiş modellerin analizleri en uzun bir saat sürmektedir. Bu açıdan bakıldığında yapılacak analizlerin amaçları doğrultusunda bu basitleştirme yöntemleri kullanılabilir. Ve bu yöntem kişiye, kaynak, para ve en önemlisi de çok yüksek miktarda zaman tasarrufu sağlayabilir.

Bu tezde tasarlanan yapının analizleri yapılırken kullanılan malzeme olarak ABS seçilmiştir. ABS katmanlı üretim teknolojilerden sıklıkla kullanılan bir plastik olmasının yanı sıra, bu tezde amaçlanan enerji emme özelliği için de uygun bir malzemedir.

Buna ek olarak, hücre yapılar da enerji emme kapasitesi yönünden yapısal olarak oldukça elverişli yapılardır. Hücre yapılar, ilerleyen kısımlarda da daha detaylı bir şekilde bahsedildiği üzere, sadece gereken yerlere malzeme konarak üretilmiş yapılardır. Yani kısaca, gözenekli ve boşluklu olarak tanımlanabilecek yapılardır. Bu sebeple, bu yapılar hafif olmalarının yanı sıra yüksek dayanım/ağırlık oranına da sahiptirler. Yani özgül enerji emme kapasitleri yüksektir. Buna ek olarak içlerindeki gözenekler ve boşluklar sayesinde yüksek deformasyon potansiyeline de sahiptirler. Enerji emme amacıyla tasarlanmış bu yapıların yüksek deformasyon özgürlüğüne sahip olmaları hayati bir özelliktir. Tabi bu deformasyonun elastik olması şartı vardır.

Bu tezde tasarlanan yay benzeri hücre yapıda ilk olarak aranan özellikler, plastik deformasyona uğramaması, yüksek deformasyon özgürlüğüne sahip olması, ve hafif olmasıdr. Ve tasarlanan yapı bu özellikler doğrultusunda dizayn edilmiştir.

1. INTRODUCTION

The production of parts and geometries, which are highly complex, are now enabled by the dramatic development of additive manufacturing (AM) technologies. Thanks to AM technology, complex structures can be produced in a cost efficient way with much less tools. Consequently, complex cellular structures started to have more attention since the manufacturability problem is no more. Being light weighted, having high energy absorption capacity, and low density are the major characteristics of cellular structures.

In this thesis a complex cellular material geometry is designed in order to have high energy absorption and impact absorption. The first chapter in the thesis is an introduction chapter to the major topics. These major topics are namely, Additive Manufacturing: where general features and methods of AM process are presented; Cellular Materials: where a brief definition of cellular structures and examples from literature are given; Purpose of the Study: where the purpose of the thesis is told; and lastly Study Plan: a walk-through to the study plan, the steps of the study period and a brief summary of next chapters.

1.1 Additive Manufacturing (AM)

Additive manufacturing (AM) is a manufacturing process, where 3D computer aided design (CAD) data is used to construct a structure by adding deposited material layer upon layer. This material can be plastic, concrete, ceramic, and metal (Gebhardt, 2012). In other words, in AM process in order to build up the given CAD data, materials are added in layers. These layers are thin cross sections of the particular CAD file. Also, 3D printing is a widely used term for AM process.

It is true that AM is an expensive process but at the end it can be easily seen that it is cost efficient (Klahn, Leutenecker, & Meboldt, 2014). Because AM does not need any workers, a lot of space, much time or any tools. And as the AM technology progresses, its cost efficiency will increase without any doubts. Despite the fact that

AM technology has been under developed for several years, day by day it is getting its deserved place in research areas and in public mind (Klahn, Leutenecker, & Meboldt, 2014).

AM is an industrially mature manufacturing process. It provides designers very high degree of design freedom. Thanks to AM, it is no longer necessary to think about Design for Manufacturing, since it provides the opportunity to manufacture almost any complex geometry (Klahn, Leutenecker, & Meboldt, 2014). One of the most novel characteristics of AM is that AM does not need any tooling. This means, the designer does not need to design with compromises in order to assist the molding or material removal processes which AM does not need. Having the freedom to design and manufacture any structure with high complexity without any designing compromises increased the popularity of complex cellular structures.

There are many AM processing techniques, namely, photo polymerization, powder bed fusion and extrusion based processes. These three are the most common processes for AM (Gibson, Rosen, & Stucker, 2015).

Photo polymerization processes, as it can be understood from its name, uses radiation curable resins and photopolymers as materials. These materials react to the ultraviolet (UV) radiaton. While the material jetting system deposits the material selectively according to the CAD data, the light source cures the layer and solidifies it.

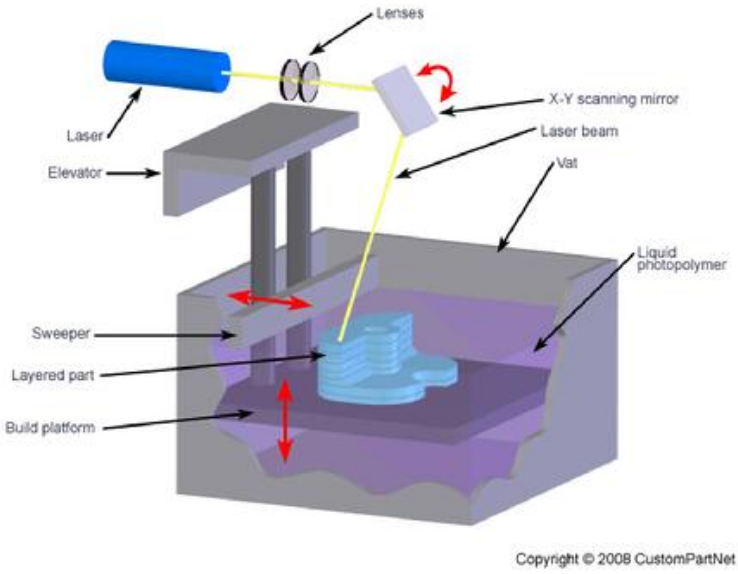

Figure 1: Photo polymerization.

Powder bed fusion (PBF) process is also a common AM technique and it is among the first commercialized AM systems. PBF is the generalized name of the process. There are many different PBF operations but all use the same basic approach. There are two or three powder beds filled with power are used in powder bed fusion based methods. By using thermal energy, the layers are made in one of the beds. In this method, when a layer is created in this bed, the bed is lowered. When the bed is lowered new powder is swept from the other onto the building bed. The differences occuring between the powder bed fusion processes are caused by different materials to be used, enhance machine productivity or avoid specific patented characteristics of the systems. The first commerialized powder bed fusion method is selective laser sintering (SLS), which is the most widely used PBF technique.

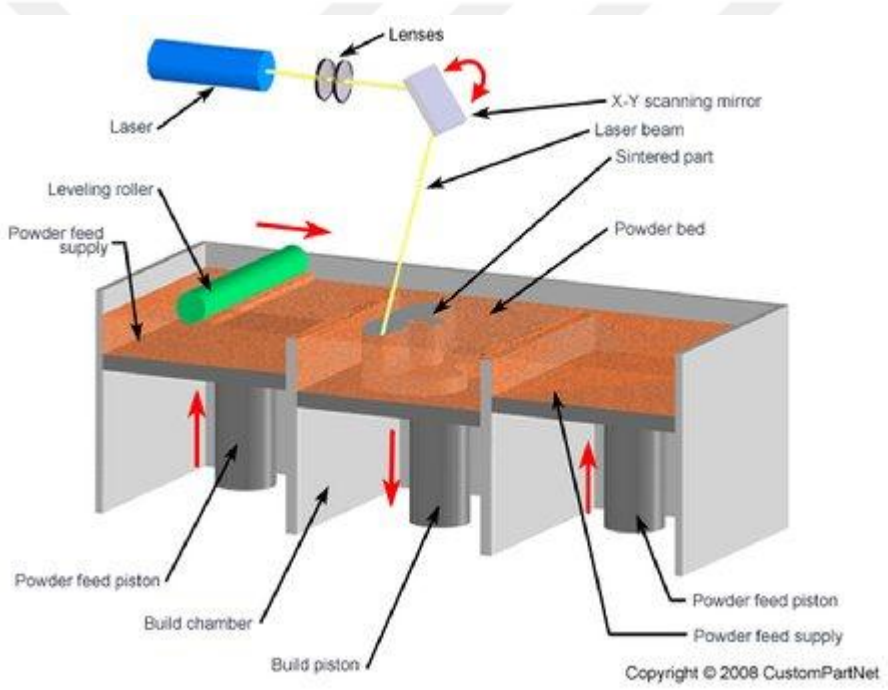

Figure 2: Powder bed fusion. Selective Laser Sintering (SLS) using a 3 bin system.

In extrusion based processes, the final structure is created by selectively depositing the material. This is done by extruding the material from a heated narrow nozzle. In this method, the material used is generally a plastic or a paste. In the cases, where a plastic is used as material, a plastic filament is fed to the hot nozzle. The small diameter nozzle is heated in order to melt the filament, so in this way the material can be deposited selectively. For paste materials, a syringe type equipment is used to deposit the paste.

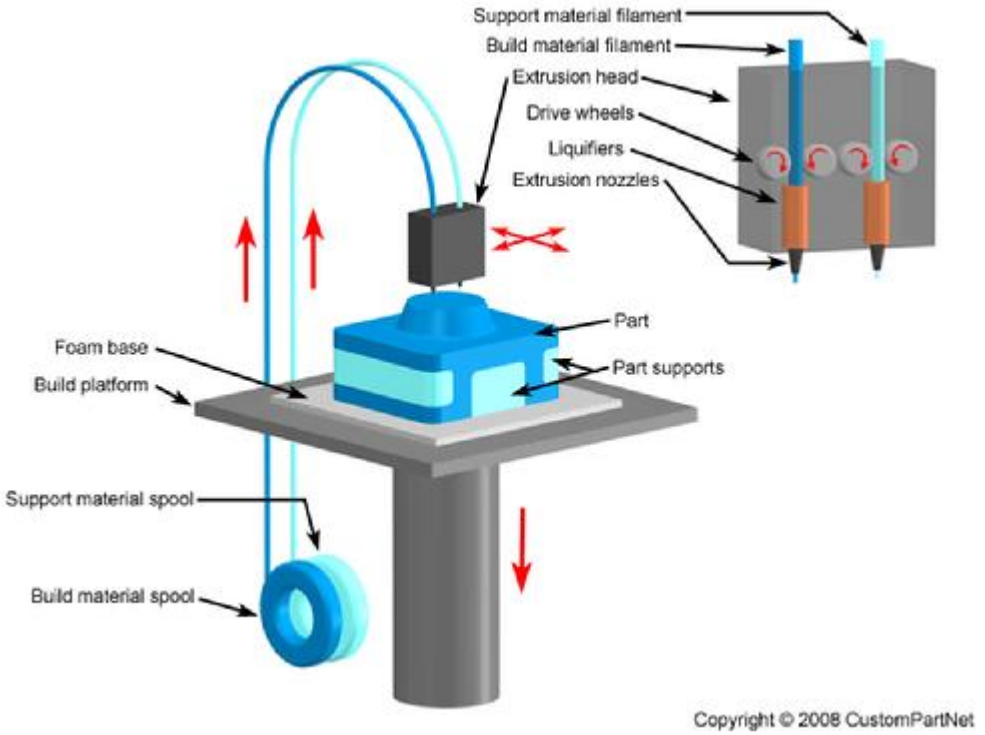

Figure 3: Material extrusion. Fused Deposition Modeling (FDM) showing the part (dark blue) and support material (light blue).

As it is mentioned above, since AM can produce structures with high complexity with giving the designer a lot of freedom increased the popularity of micro and macro level cellular structures.

1.2 Cellular Structures and Literature Review

The cellular material concept is formed by the idea of putting material only where it is needed. The needed places vary by the application, where the cellular material will be used. By using materials only where it is needed, it can be easily said that cellular materials offer high strength with a relatively low mass. Cellular materials provide high energy absorption properties and can be used as good thermal and acoustic insulators (Gibson & Ashby, 1997).

Cellular structures are the basis of this thesis. These materials can be found in nature and as well as can be manufactured by humans. Cork, wood, honeycomb and cancellous bone structures are good examples of natural cellular structures. Human-made cellular structures are foams and some structures which are imitated from nature such as honeycombs. Both of these natural and human-made cellular structures have a common characteristic, which is their microstructure consists of

interconnected network of struts or plates. The cells, that consists of interconnected network of struts are called open-cell structures, where the cells consisting of interconnected plates are called closed-cell structures. The cellular structure designed for this thesis is a open-cell cellular structure (N. Michailidis, 2010).

Almost any kind of material can be fabricated into cells. The most common material to be used is polymers and plastics, of course. But also metals, ceramics, glasses and composites can be functioned as cellular structures. In the figures below, some kinds of cellular structures are presented (Gibson & Ashby, 1997).

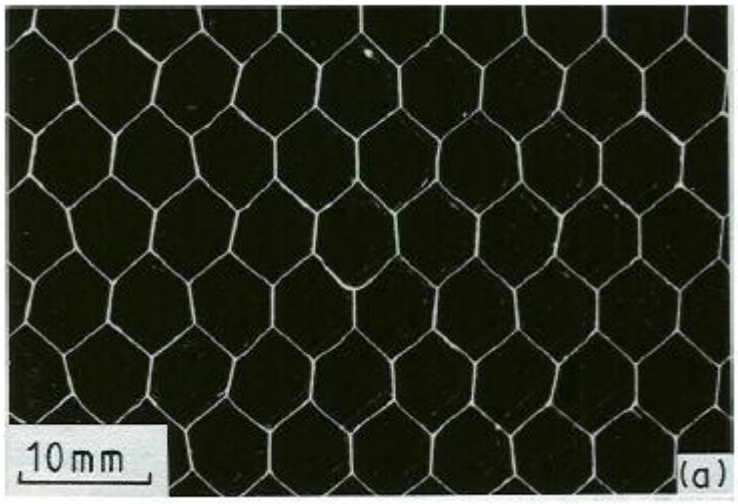

Figure 4: 2D honeycomb cellular structure (Gibson & Ashby, 1997).

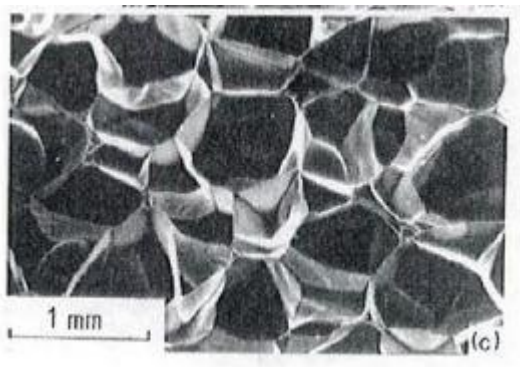

Figure 5: 3D foam with open-cells (Gibson & Ashby, 1997).

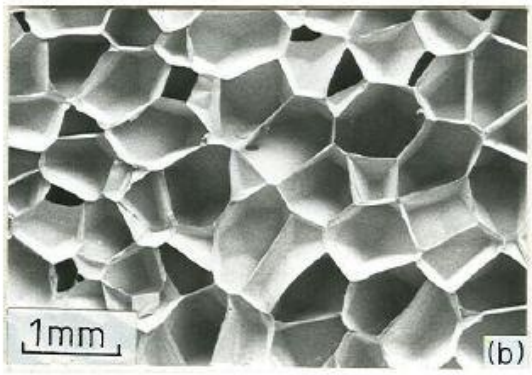

Figure 6: 3D foam with closed-cells (Gibson & Ashby, 1997).

A cellular structure's mechanical properties do not only depend on the materials it is made. The micro-morphology of the cellular structure, spatial distribution of the cells, the size and the shape of the cells are also vital parameters for mechanical properties of a cellular structure (Nguyen & Noels, 2014). To define the mechanical properties of cellular structures, the relative density and the relative elastic modulus of the structure are what we count on (F.Ashby, M., J.Gibson, L., Evans, A., Fleck, N., Hutchinson, J., & Wadley, H., 2000).

Polymeric, plastic, ceramic or metallic cellular structures are appealing alternatives to manufacture light weight and stiff materials. Crash and impact protection is one of the best application for those light weighted stiff structures, where these application ranges from acoustic and thermal insulation packings to crash protection (S.K. Nammi, 2010).

Since having high energy absorption potential, crash protection potential and impact protection potential are important aspects of cellular structures; there are many designs published in the literature. Among those designs, there are truss lattice structures. Truss lattice structures are open-cell human-made cellular structures. They are connected with each other with an hierarchical order. In such works, a parametric finite element study is held in order to find the optimal relative density and cross section. Static and dynamic analysis are made in order to find those parameters. In a particular study, an octet truss lattice structure is designed and the effect of those parameters are studied (T. Tancogne-Dejean, A. B. Spierings, D. Mohr, 2016). In this study it is found that 30% relative density stainless steel 316L basis material octet truss lattice structure has a higher specific energy absorption than the conventional hexagonal honeycomb (T. Tancogne-Dejean, A. B. Spierings, D. Mohr, 2016).

In another study, a stainless steel cellular lattice structure, which is manufactured by selective laser melting (SLM) method, is designed. In this study the compression strength and compression modulus of the designed lattice structure are calculated and compared with the ones with different parameters. It is found that these properties of the lattice structure increase as the volume fraction increase (C. Yan, L. Hao, A. Hussein, P. Young, D. Raymont, 2013).

Cellular sandwich panels are also another area to use cellular structures. In a particular study, sandwich samples of various designs are manufactured. These designs are re-entreant auxetic, rhombic, hexagonal and octahedral shaped designs where nylon 12 is used as material and manufactured by SLS. Energy absorption potentials of these various designs are compared. Also the effects of manufacturing issues like, geometrical accuracy and anisotropy on the energy absorption performance are discussed. In this study it is found that the different shapes of mentioned cellular structures in sandwich panels demonstrate significantly different low-energy drop weight impact characteristics. The hexagonal sandwich structure has the largest compliance with the smallest energy absorption capacity where the octahedral sandwich panel has high stiffness with good impact protection capacity. Also, it is found that the re-entrant auxetic sandwich panel design could be used as a good high energy absorber with low response force if a proper geometrical design is made. These characteristics of the design makes it very attractive for low-energy drop weight impact protection applications (Li Yang Ola A Harrysson Harvey A West II Denis R. Cormier Chun Park Kara Peters, 2015).

In another study, a periodic cellular lattice structure designed and manufactured with direct metal laser sintering (DMLS) method where an aluminum alloy is used as material. This study assesses the manufacturability and performance of $AlSi_{10}Mg$ periodic cellular lattice structure. The repeated unit cell is named “diamond” in this study. Since the “diamond” unit cell is self supported, peroidoic cellular structures with low volume fraction (7.5 – 15%) can be fabricated with DMLS method where the unit cell size range is 3 mm to 7 mm. It is found that there is a clear relation between the compressive modulus and strength, and volume fraction and unit cell size. In general, this study shows that with DMLS, it is possible to manufacture light-weight aluminum periodic cellular structure with controlled size and volume fraction with the predicted mechanical properties easily (C. Yan, L. Hao, A. Hussein, S. L. Bubb, P. Young, D. Raymont, 2013).

Among those cellular structures, there are also much smaller lattice structures, which are called nanolattices. There is also a study to approach theoretical strength of glassy carbon nanolattices (J. Bauer, A. Schroer, R. Schwaiger, O. Kraft, 2016). The approached structure has struts shorter than 1 μm and diameters as small as 200 nm. They represent the smallest lattice structure yet produced. The structure achieves a material strength of a up to 3 GPa, which corresponding nearly to the theoretical strength of glassy carbon. The strength – density ratios of similar microlattices have six times lower than this model. By using a honeycomb topology the effective strength of a 1.2 Gpa at 0.6 g cm^{-3} is achieved where diamond is the only bulk material with a higher strength – density ratio (J. Bauer, A. Schroer, R. Schwaiger, O. Kraft, 2016).

Since it is known that cellular materials are triumphant in impact absorbing and light-weighted, they are extremely attractive for head protection applications. There is a study that focuses on head impact protection. In this mentioned work, a previously designed and tested design concepts are adapted to application-based environments. The aim on this study is contouring previously-planar structures into hemispherical (head) geometry, while retaining the mechanical performance (S. Soe, W. Jabi, P. Theobald, 2016). This design inspired the unit cellular structure designed for this thesis.

In another study the hierarchical bio-cellular structure of luffa sponge is mimicked in order to design a hierarchical foam cylinder reinforced by stiff thin-walled carbon fiber reinforced plastic (CFRP) tubes. Luffa sponge is a natural hierarchical bio-cellular structure with pores in macro and micro scales. The strength of the luffa sponge is enhanced dramatically by its stiff inner-surface layer around the macro pores. In this study, the compression behaviour of the cellular structure, which mimicks the luffa sponge, is found. It is seen that the specific energy absorption (SEA) of the designed hierarchical structure is dramatically higher than the pure aluminum foam cylinder (X. An, H. Fan, 2016).

In another paper published in 2013 studied the polyurethane foam filled pyramidal lattice core snadwich panels. This structure is fabricated in order to increase the energy absorption resistance. From the compression tests, it is seen that the foam filled sandwich panels have a larger load carrying capacity when it is compared to the unfilled specimens. In addition, the energy absorption efficiency of foam filled structure with higher relative density is lower than the unfilled structures. This results

are valid when the compressive strains is small. It exhibits well when the compressive strain is around 0.25, and the performace increases as the compressive strains increases. On the other hand, foam filled structures with lower relative density have lower energy absorption level when it is compared to the unfilled specimens. Lastly, but not least, this paper reveals that during the low velocity impact tests the contact duration for foam filled specimens is shorter and peak load has a slight increase (G. Zhang, B. Wang, L. Ma, L. Wu, S. Pan, J. Yang, 2013).

Lastly, but not least, in a study made in 2012 investigates the potentian of AM lattice structures for impact absorption. This study focuses on conformal body protection. Two different designs are compared in this paper and it is seen that the cellular structure with helical struts performs much better than the structure with straight struts. Even it is not the main focus to find out this difference, it gave inspiration for the design which is made for this thesis. The reason behind the helical design is, the helical struts increases the overall length of the design, which means more deformation freedom in both directions (compression or tension). Thanks to allowing more deformation it is easy to say that the helical design absorbs more energy. Both of the designs can be seen in the figure below (J. Brennan-Craddock, D. Brackett, R. Wildman, R. Hague, 2012).

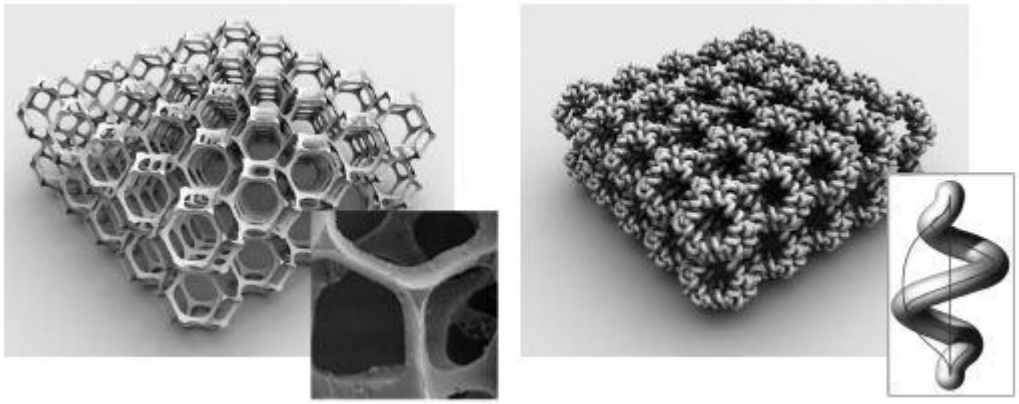

Figure 7: Straight-strut structure and helical-strut structure (J. Brennan-Craddock, D. Brackett, R. Wildman, R. Hague, 2012).

1.3 Design Method

The design method consists of three main steps. The first step is unit cell design, where the unit structure is designed. In this thesis as the CAD sofware Solidworks is used. After the first step, in order to find out how the unit design behave under certain cirumstances, simple static FEM analyses are made in Abaqus CAE.

In the second step, the design is modified until the static analysis results give favorable data. The second step is like a loop until design gets optimized with modification for the application. After the basic concept of the unit design is done, the second step is repeated for different parameters like cross section area, strut shape etc. All these results are noted and used to see that how each parameter affects the design.

The third and the last step of the design method is construction. In this step the optimized unit cellular structures are connected with each other hierarchically. This connected design is put between two plates in order to build a sandwich structure.The design method can be summarized with a simple outline, which is given below.

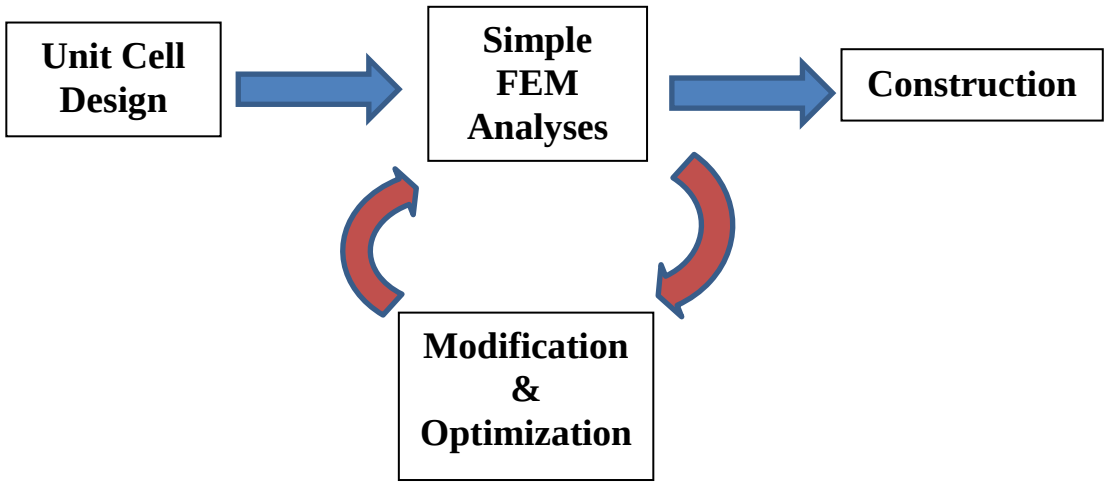

Figure 8: Design method.

When the unit cell design is completed, optimized and constructed the design process is done.

After that it comes to analyze the structure dynamically in order to find the specific energy absorption data with more complicated FEM analyses. For this thesis,

material is chosen to be Acrylonitrile Butadiene Styrene (ABS) since the structure is designed to manufacture with AM. The material properties for ABS for AM processes are investigated in a particular study and the resulting data are used for this thesis. (J. Cantrell, S. Rohde, D. Damiani, R. Gurnani, L. DiSandro, J. Anton, A. Young, A. Jerez, D. Steinbach, C. Kroese, P. Ifju, 2017).

1.4 Purpose of The Study

In this thesis, the purpose of the study is designing a closed-cell cellular structure with high specific energy absorption. It is known and mentioned in previous chapters that additevely manufactured cellular structures have beneficial energy absorbing characteristics. For this purpose, the designed unit cell structure should deform without yielding. In order to achieve this goal, helical struts are used, which provides longer overall length for the structure and letting the model deform freely without yielding. As the model has a higher range of elastic deformation freedom, it can be said that the model will absorb more energy (J. Brennan-Craddock, D. Brackett, R. Wildman, R. Hague, 2012).

Being in elastic region while deforming is a key characteristic for the model. Because when the yield point is exceeded, the design will no longer expand back to its original shape. In the dynamic analysis of the constructed sandwich model, a rigid plate squeezes the model with a certain instantenaous velocity.

The expectation from the model is absorbing the rigid plate’s kinetic energy, stop it, and lift it back while expanding to its original shape. That is why the model should not yield while crashing by the rigid plate. The energy absorbed is caluclated by referencing the plate’s velocity during analysis. The maximum energy of the rigid plate is at the beginning of the analysis. As the rigid plate starts to squeeze the model, it slows down. Until it stops, the model continues to absorb kinetic energy. After the rigid plate stops, the model lifts the rigid plate proportional to its amount of absorbed energy.

In static analyses, which are made for optimizing the unit cell, aims to minimize the maximum stress under same deformation. The parameters of the design is changed to see how the model reacts with the same deformation level. So, the effects of the

parameters are also studied and can be found in next chapters. The details of the static and dynamic analyses are also presented in the next chapters.

To summarize, in this thesis a closed-cell cellular structure is designed. This cellular structure is designed to have high deformation freedom without yielding, which is an important aspect of energy absorpant materials. Like it is said in previous sections, high deformation freedom helps to ensure good energy abosrbing qualities (J. Brennan-Craddock, D. Brackett, R. Wildman, R. Hague, 2012).

In the following section, how the unit cell is designed is explained, the details of the design, how it is assembled and the construction process is presented.

To assmeble the unit cell, first a spring-like element is designed, and these spring-like elements are assembled into the unit cell structure. After that when the unit cell design is done, construction of the sandwich structure is made.

2. DESIGN OF THE SPRING-LIKE CELLULAR STRUCTURE

As it is mentioned in Design Method section, the modelling starts with the design of the unit cell. The unit cell is designed in Solidworks CAD software. At first the design of the unit cell and its parameters are discussed. After that section, the optimization of the unit cell and the effects of each parameter is presented. Lastly, the construction of the sandwich structure is explained.

2.1 Design of The Spring-Like Unit Cell

The unit cell designed for this thesis consists of 4 circular spring-like elements with helical struts. One circular element can be seen in the figure below:

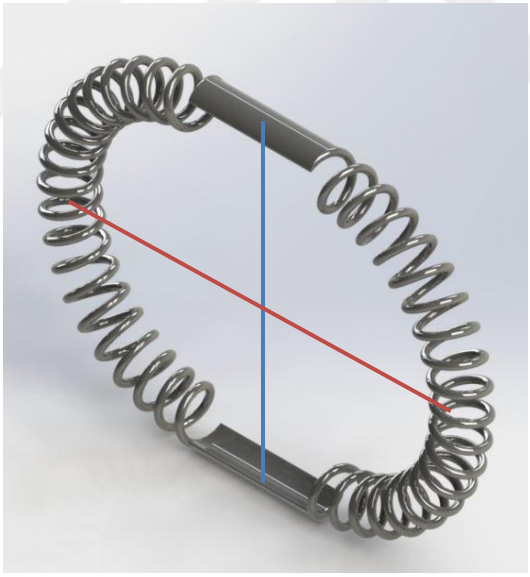

Figure 9: Circular spring-like element with helical struts.

These circular spring-like elements are assembled to the unit cell, in a way that their vertical axes (the blue line in Figure 9) are coincident and the consecutive horizontal axes (the red line in Figure 9) make 45 degrees with each other.

So, after the assembly of the four spring-like circular elements, in an order that explained in previous paragraph, the unit cell design looks like in the following figure.

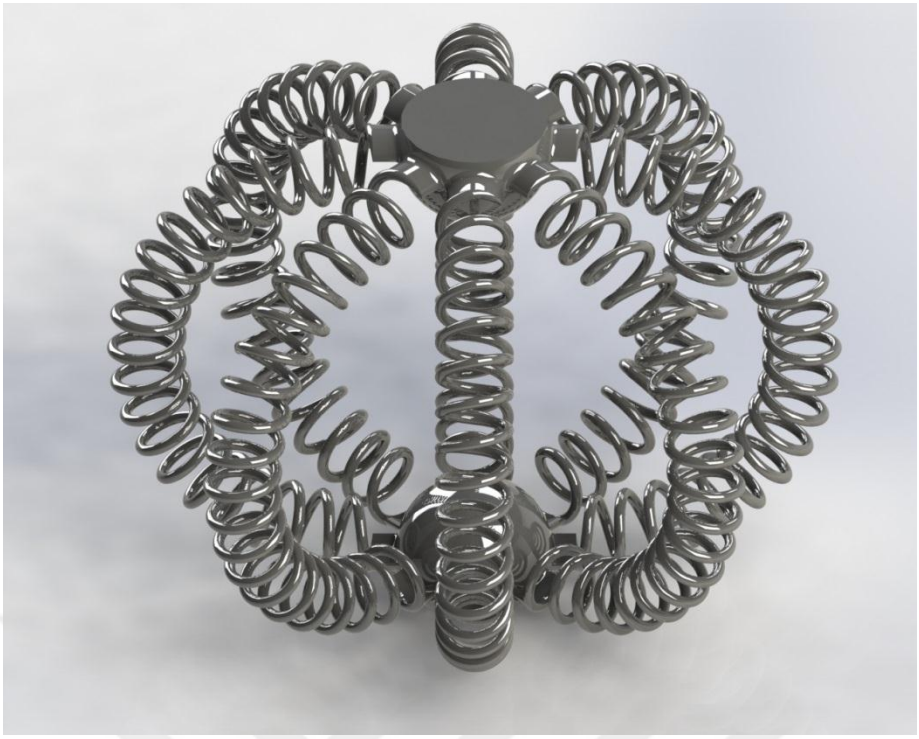

Figure 10: Unit spring-like cellular structure.

In Figure 10, the main concept of the unit cell can be seen. Between Figure 9 and Figure 10 there is a difference at the top and at the bottom of the design. In Figure 9, it can be clearly seen that there are non-helical segments in the part, which are placed where the blue line starts and ends. The reason is, when the circular element in Figure 9 is assembled into the unit cell there would be geometrical complexities at the top, and at the bottom due to helical struts, which would make the design inferior against all kind of deformation. So to make a smoother intersection for circular spring-like elements in the assembly, a half sphere is placed at both of the inersection points. Also these half spheres makes the vertical connection between unit cellular structures in the construction phase.

In the next step, as it is mentioned in the Design Method section, the optimization will take place. Determining the parameters, seeing each parameter's effects on the design will be presented in the next chapter.

2.2 Parameters of The Spring-Like Unit Cell

To optimize the unit cell design, first the parameters should be determined. For this design, three main parameters are considered, namely; cross section diameter, turn radius, and number of turns.

Cross section diameter is the diameter of the circular cross section of the helical struts. Turn radius is the raidus of helices for each turn the helices make. And lastly, the number of turn is the number of circles that the model makes with helices for each circular element, which is shown in Figure 8. These parameters can be understood more clearly in the figures below:

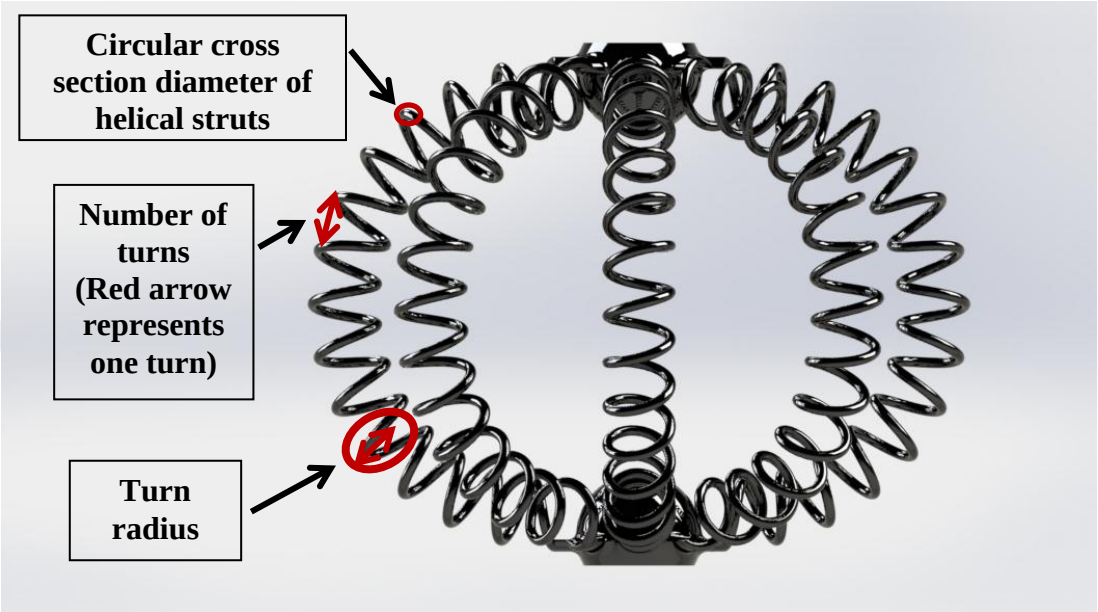

Figure 11: Unit element with helical struts with parameters shown on it.

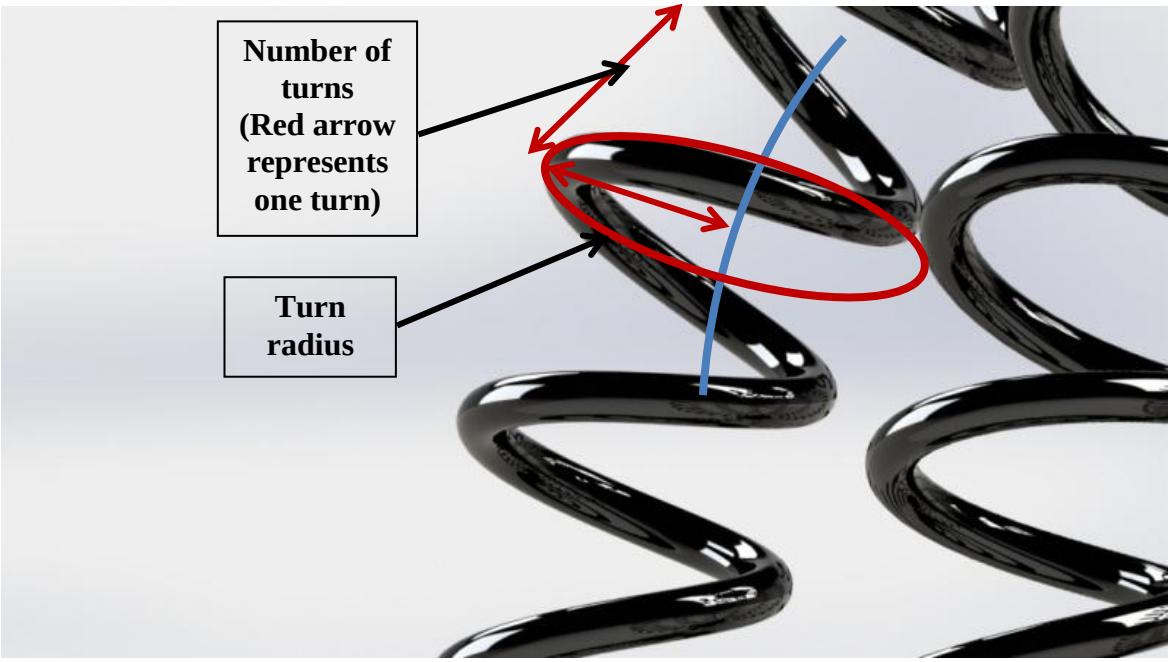

Figure 12: A closer look to the helical struts to clearify the turn radius and number of turns.

2.3 Construction of The Sandwich Structure

As it is mentioned in Design Method section, the last step of the design process is the construction. After the optimization process is done, one should assemble the unit cellular structures into a sandwich structure. To do that, a vertical and a horizontal connection must be specified. After these connections are decided, the whole model is put between to plates in order to assemble it to a sandwich structure. In this section, the connections between the unit cellular structures are explained.

The vertical connection used for the assembly is very simple. While designing the unit cellular structure two half spheres are used to get rid of the geometrical complications. These half spheres are also used for the vertical connection in this step. Since they are identical for each model, they match each other perfectly if one of them is put on another one. So for the vertical connection no extra connection part is used, and two unit cellular structures are simply connected via these half spheres. To summarize, one unit cellular structure is put on another one.

The horizontal connection for the assembly is also a simple one. The imbricated unit cellular structures, which are mentioned in previous paragraph, are placed next to each other with a certain distance. So it can be said that the unit cellular structures do not have a horizontal connection with each other. In other words there is no contact between horizontally placed unit cellular structures. But the distance specified for the placement is done with a certain manner, which prevents any contact when the sandwich structure is compressed and expanded horizontally. So simply it can be said that there is no specific horizontal connection between the unit cellular structures. The only things that connects the imbricated unit celullar structures horizontally are the top and lower plates of the sandwich structure.

In the Figure 13 in the next page, the sandwich structure can be seen.

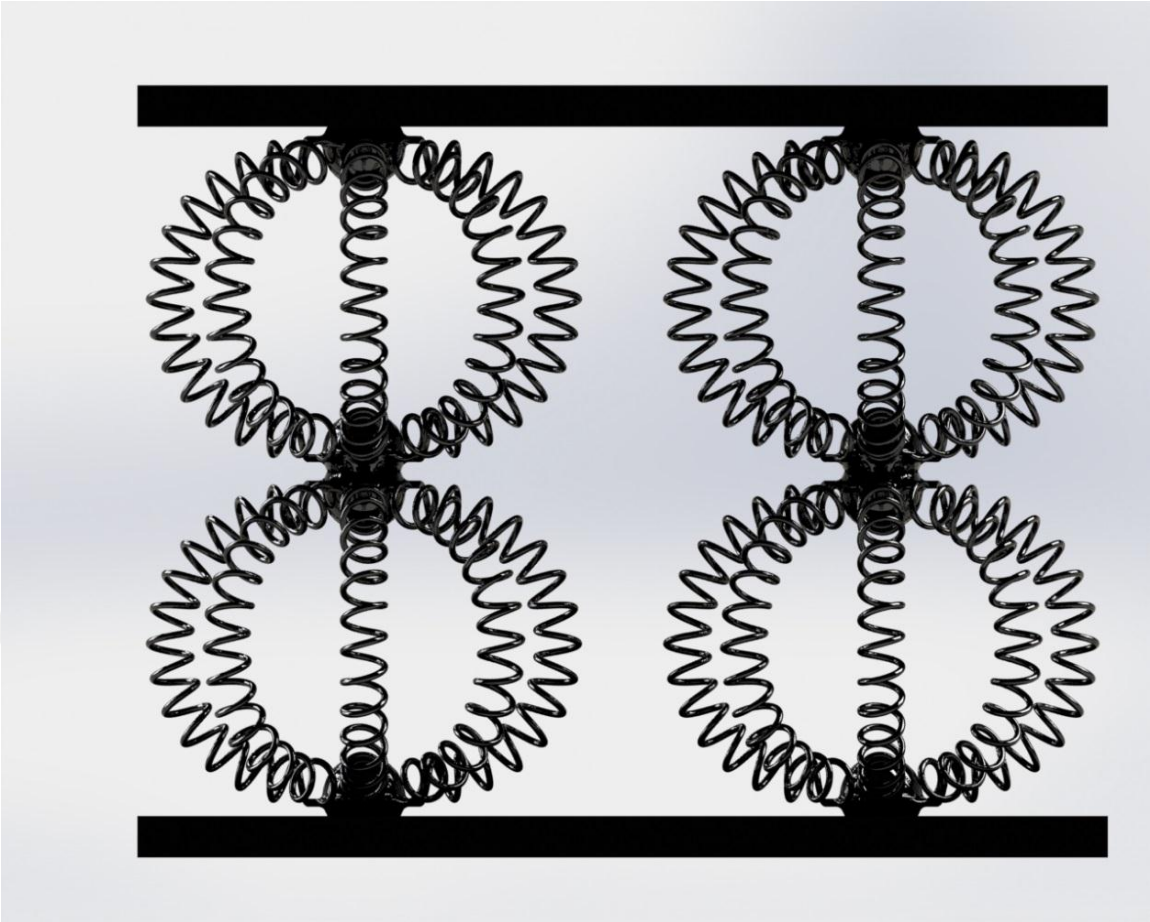

Figure 13: 4x2 Sandwich structure from front view.

As it can be seen in the figure above, the unit cellular structures does not have any connections. And, even the part highly deforms, the struts do not touch each other. A construction method like this is chosen to ensure the deformation freedom in order to protect the energy absorbing qualities of the sandwich structure. As it is mentioned previously, the only horizontal connection in this structure is made my the top and lower sandwich plates which can be observed in the figure above.

3. NUMERICAL MODELLING AND ANALYSIS OF THE CELLULAR STRUCTURE

In this section the finite element (FE) modelling of the sandwich structure and the results will be presented. For the sandwich structure, which can be seen in Figure 13, will be used for the analysis. In the corresponding sandwich structure there are 8 unit cellular structures. It has 4 unit cellular structures on the first floor and 4 on top of them. Firstly, a bunch of simple finite element analyses are run to see the effects of the parameters which mentioned in previous chapter. Secondly, an explicit dynamic analysis is run to see the model's energy absorption capabilites. The software used is Abaqus CAE. In next chapters, effects of the parameters, details of the analyses, material properties, boundary conditions and initial conditions for each analysis will be presented. In addition a brief explanation FEM and dynamic explicit analyses will be given.

3.1 Finite Element Method (FEM)

Finite element method (FEM) is a numerical method to solve highly complicated problems, which cannot be solved satisfactorily with analytical solutions. These problems can be stress analysis problems, heat conduction problems etc. This method solves many algebraic equations simultaneously, to find the results. To solve these algebraic equations, digital sources like personal computers, mainframes and all other sizes between are used. It should be mentioned that, FEM results are rarely exact. But still, the results are accurate enough for engineering purposes and highly efficient in means of time and cost. Also, it is possible to decrease the error percentage by solving more algebraic equations simultaneously (R. D. Cook, 2002).

In the following figure, the *discretization* process, which is a basic finite element concept, is shown on a very simple problem.

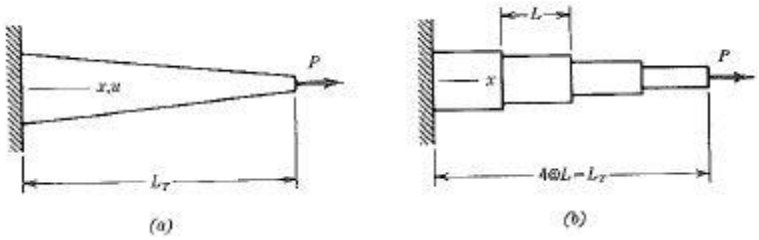

Figure 14: (a) A tapered bar under end load P. (b) A model built of four uniform (non-tapered) elements of equal length (R. D. Cook, 2002).

It is known that, in the classical analytical approach, to solve this problem the differential equation must be written and solved. However, the finite element approach to this simple problem does not begin with a differential equation. Instead of it, the problem is discretized as it can be seen in the figure above, and modeled as series of *finite elements*, which are uniform but with varying cross sectional area. For each finite element, the elongation changes, because the cross section are changes as x (horizontal position vector) increases. The elongation of each element can be calculated by the simple formula, PL/AE. And it is known that at the end of the bar, the elongation equals to the sum of the element elongations. As the number of finite elements are increased, the result is improved and, the error is lowered (R.D. Cook 2002).

3.2 Simple Finite Element Analyses for Modification and Optimization Step

To determine how the parameters, which are shown in previous chapter, a bunch of simple finite element analyses (FEA) are made. In these analyses, the unit spring-like cellular structure with specific parameters is exposed to a certain displacement. The displacement is applied to the top surface of the model, while the bottom surface's boundary condition is defined as encastre. The spring-like unit cellular structure has a sphere-like shape with a diameter of 100 mm. The all unit cellular structures with different parameters are exposed to the same displacement in negative y direction, which is 15 mm. For all three parameters, at least three analyses are run. For example, to see the effect of the cross section diameter all other parameters are held constant and the cross section is changed.

To understand the analysis more clearly, the following figure can be seen.

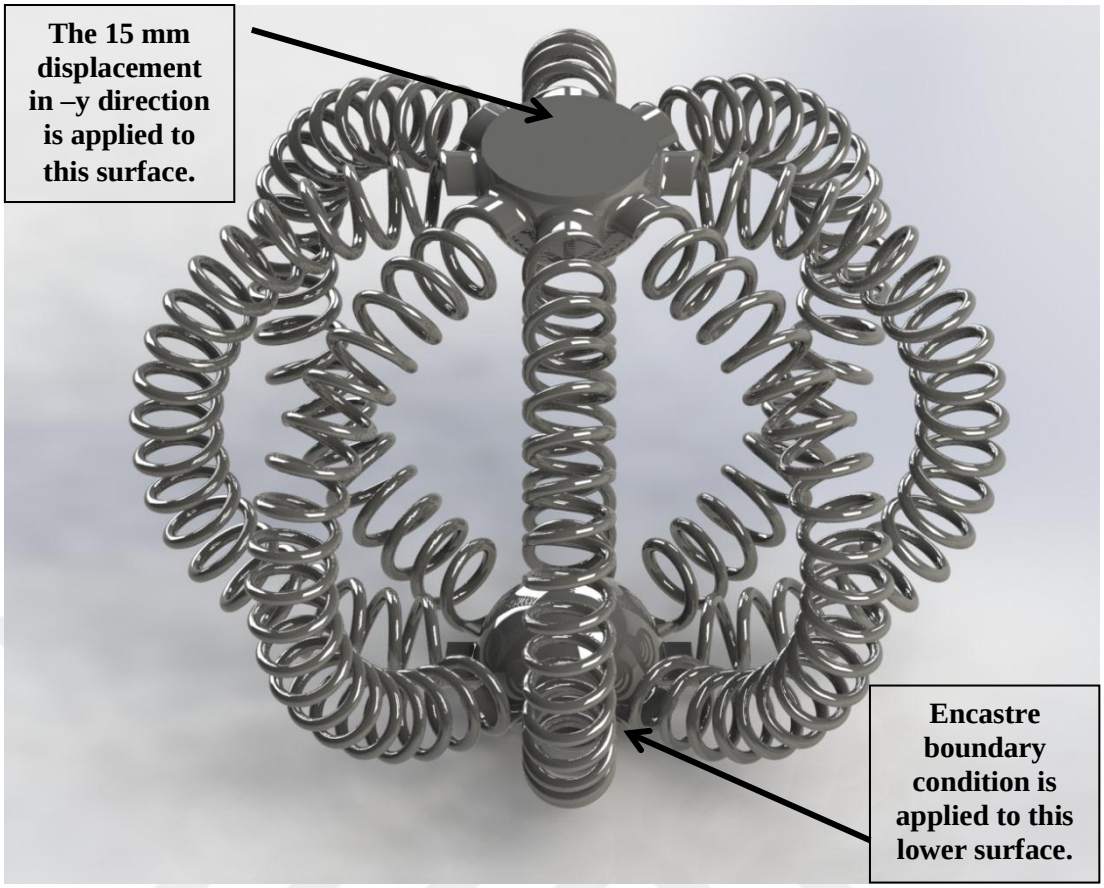

Figure 15: The spring-like unit cellular structure with the applied boundary conditions.

First of all, the effect of cross section diameter of the struts is investigated. To see that, three analyses are run where the cross section diameter changes and the other two parameters stay constant. The most vital results from these analyses are the maximum stress values occuring in each model. Since yielding is not wanted in the design, the aim here is to lower the maximum stress as much as possible.

Since the material is chosen to be ABS, the maximum stress value should be lower than 30,4 MPa, which is the yield limit of ABS (J. Cantrell, S. Rohde, D. Damiani, R. Gurnani, L. DiSandro, J. Anton, A. Young, A. Jerez, D. Steinbach, C. Kroese, P. Ifju, 2017).

In the following table, the effect of the cross section diameter on the maximum stress value can be seen.

Table 1: Effect of cross section diameter on maximum stress value.

STATIC ANALYSIS (-15 mm DISPLACEMENT)				
CROSS SECTION DIAMETER CONTROL				
	Cross Section Dia (mm)	**Turn Radius (mm)**	**Number of Turn**	**Maximum Stress (MPa)**
Model 3	2,5	2,5	52	25,50
Model 1	3,75	2,5	52	27,87
Model 2	5	2,5	52	36,90

From Table 1, it can be clearly seen that as the cross section diameter increases, the maximum stress observed in the model also increases. While for Model 1 and Model 3 maximum stree-ss values are lower than the yield limit, for Model 2 it exceeds the yield limit. Despite of the fact that, Model 3 and Model 1 maximum stress values are lower than the yield limit, they are not beneficial enough for this application. Since the applied displacement is only 15 mm and it is just around the 15% of the model height, it will not be wrong to say that these model will also yield with a slightly higher displacement. And it is obvious that while doing the explicit dynamic analysis for energy absorption, it will be exceeded. So by changing the other two parameters, lowering the maximum stress value is a must.

Secondly, the effect of turn radius is investigated. As it is done in previous parameter investigation the other parameters are held constant. In the following table the effect of the turn radius on the maximum stress value can be found.

Table 2: Effect of turn radius on maximum stress value.

STATIC ANALYSIS (-15 mm DISPLACEMENT)				
TURN RADIUS CONTROL				
	Cross Section Dia (mm)	**Turn Radius (mm)**	**Number of Turn**	**Maximum Stress (MPa)**
Model 3	2,5	2,5	52	25,50
Model 4	2,5	5	52	9,30
Model 13	2,5	7,5	52	8,22

From the data given in Table 2, it can be clearly seen that as the turn radius increases, the maximum stress value decreases. Between Model 3 and Model 4 a dramatic decrease is observed in maximum stress data. So it can be said that turn radius has a critical role in this design concept. But also, if Model 4 and Model 13 is compared there is no great difference in maximum stress values. So it can be said that, after one point models do not react much to this paremeter. But still, the dramatic change between Model 3 and Model 4 for maximum stress data makes this parameter a vital one.

Lastly, the effect of turn number is investigated. As in the previous parameter investigations, other parameters are held constant and turn number is changed to see its effect on maximum stress value. In the following table the effect of turn radius on the maximum stress can be seen.

Table 3: Effect of turn number of maximum stress value.

STATIC ANALYSIS (-15 mm DISPLACEMENT)				
NUMBER OF TURN CONTROL				
	Cross Section Dia (mm)	**Turn Radius (mm)**	**Number of Turn**	**Maximum Stress (MPa)**
Model 4	2,5	5	52	9,30
Model 14	2,5	5	40	10,88
Model 9	2,5	5	28	11,96

From the data presented in Table 3, it can be seen that as the turn number decreases, there is a slight increase in maximum stress data. But since maximum stress values for these models are very close to each other, it is not possible to determine the turn radius effect clearly. To clarify the effect, another investigation is made.

For the second investigation for the parameter turn number, one of the parameters which is held constant is changed. This parameter is chosen to be the turn radius and held constant on 7,5 mm this time. Also it should be mentioned that, this choice is made arbitrary. The table presenting the second investigation's results for turn number parameter can be seen in the following table.

Table 4: Effect of turn number on maximum stress value (2).

STATIC ANALYSIS (-15 mm DISPLACEMENT)				
NUMBER OF TURN CONTROL (2)				
	Cross Section Dia (mm)	**Turn Radius (mm)**	**Number of Turn**	**Maximum Stress (MPa)**
Model 13	2,5	7,5	52	8,22
Model 15	2,5	7,5	40	8,97
Model 10	2,5	7,5	28	6,78

From the data presented in Table 4, the effect of the turn number is still ambigious. The maximum stress data have close values similar to the data in Table 3. Also, again there is no clear increase or decrease in maximum stress data as turn number decreases. So, the model's major parameters that affect the maximum stress value determined as the cross section diameter and turn radius. But it does not mean that number of turns does not affect the design for this application.

Maximum stress value is one of the vital values to investigate, but not the only one. For the design and optimization process lowering the maximum stress is the main goal, so for the simple FEM analyses only the maximum stress value is considered as a design criterion. But it can be seen in the next chapters that, especially for the explicit dynamic analysesi equivalent stiffness constants of the models are also calculated which is an essential criterion. The reason it is calculated and the resultant values are presented in the next chapters.

3.3 Explicit Dynamic Finite Element Analyses

Explicit dynamics is a numerical technique for calculating the equations of motion through time. It is also known as the forward Euler method or central difference method. Explicit dynamics provides the capability to solve high speed-short duration dynamics problems, large nonlinear and quasi-static problems, highly discontinuous postbuckling and collapse simulations, structural acoustics etc.

The analysis which has to be run for this thesis is a high speed-short duration analysis. In this analysis, the sandwich model will simply be crashed by a rigid plate with a certain mass and an initial velocity. The rigid plate will squeeze the model and as time passes the model will absorb its kinetic energy. After enough time, the rigid plate will slow down and stop when its all kinetic energy is absorbed by the sandwich structure. Later on the model will begin to rise the rigid plate while it expands. The analysis is repeated for different inital velocities and for different models. Three different inital velocities are specified for the analyses, 1 m/s, 4 m/s and 8 m/s. Also three different models chosen for this analyses according to their maximum stress value, which is presented in previous chapter, and their equivalent stiffness coefficinet, which will presented in the next chapters in detail.

3.3.1 Stable Time Increment In Explicit Dynamics

The explicit dynamics method solves all problems as a wave propagation problem. In this kind of problems, the unbalanced forces are propagated as stress waves between consecutive elements (R. D. Cook, 2002). A solution can be obtained if only the time increment is less than or equal to the stable time increment. If else, the solution will not be stable. Simply, the stable time increment is the minimum time that a dilatational wave gets across to the smallest element dimension in the model, and the time increment used for an explicit dynamic analysis should be lower than or equal to this value. So if there are very small elements in a model, the stable time increment will be very small, which is not desired. Because the stability limit for the central-difference method is closely related to the smallest element dimension in the model. It means that, if the mesh contains small elements, or the wave propagation speed is high, the resulting stable time increment will be very small, and the analysis will take very long time. The stable time increment depends on the dilatational wave speed, which can be calculated as:

$$c_d = \sqrt{\frac{E}{\rho}}$$

Where c_d is the dilatational wave speed, E is Young's modulus and ρ is the material density.

Also the model has a characteristic element length which is L^e. The wave speed and the characteristic element length has a direct effect on the stable time increment, which is calculated as:

$$\Delta t = \frac{L^e}{c_d}$$

So, from the formula given above one can say that decreasing L^e and/or increasing c_d will decrease the value of the stable time increment. To have a larger stable time increment in order to decrease the analysis time the followings can be done:

- Increasing element dimensions in order to increase L^e
- Decreasing material stiffness in order to decrease c_d
- Increasing material compressibility in order to decrease c_d
- Increasing material density in order to decrease c_d

Since it is not possible to change the material properties, increasing c_d is not doable. Mass scaling can be applied to increase c_d. It is a method, which adds extra mass to the specific elements in order to increase c_d value. In this thesis, mass scaling is not used since it can affect the results a lot. Thus, the only parameter it can be changed in order to increase stable time increment is L^e. It can be easily seen that, the model studied in this thesis have very thin struts. And from the parameter investigations it is obvious that as the struts go thinner, the maximum stress value decreases. So with thinner struts, the model becomes better for energy absorption because it will have more deformation freedom. But in the other hand, as it is explained above, with thinner struts there will be small elements in the 3D mesh. So there is no sufficient freedom for increasing L^e.

Since increasing the stable time increment for the model is not doable according to the reasons presented above, to decrease the analysis time another solution is found. To make it happen, the model is simplified for the explicit dynamics analysis. As it is explained before, it can be said that in this analysis the model acts like a spring. It is compressed by the rigid plate, absorbs energy, stores it and later on realeses it in order to rise the plate. So, in order to simplify the analysis, the equivalent stiffness coefficients of each model are calculated. And for the analysis, an analytical spring is

placed between the sandwich plates. The calculation method of the stiffness coefficient, and their values for each model is presented in the next chapter.

3.3.2 Equivalent Stiffness of The Sandwich Structures

To calculate the equivalent stiffness of a single cellular structure, the static analyses used for the optimization step are used.

The reaction force at the bottom of the models are measured and plotted with the corresponding displacement values. Since multiplying the displacement by the spring constant gives the reaction force, the slope of the corresponding graph's linear trendline gives the equivalent stiffness coefficient of the model. For each model, this value is calculated. And to choose three models for explicit dynamic analysis, in addition to the maximum stress value the equivalent stiffness is also considered. The reaction force v displacement graphs of each model and their equivalent stiffness values can be found in the following pages.

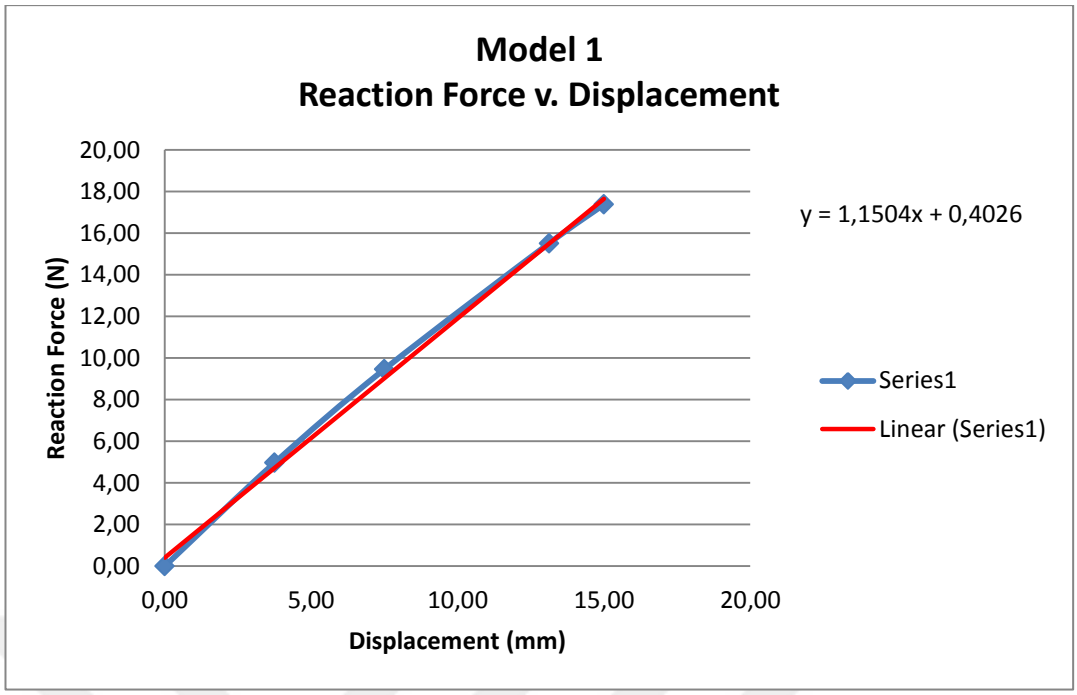

Figure 16: Reaction Force v Displacement graph for Model 1.

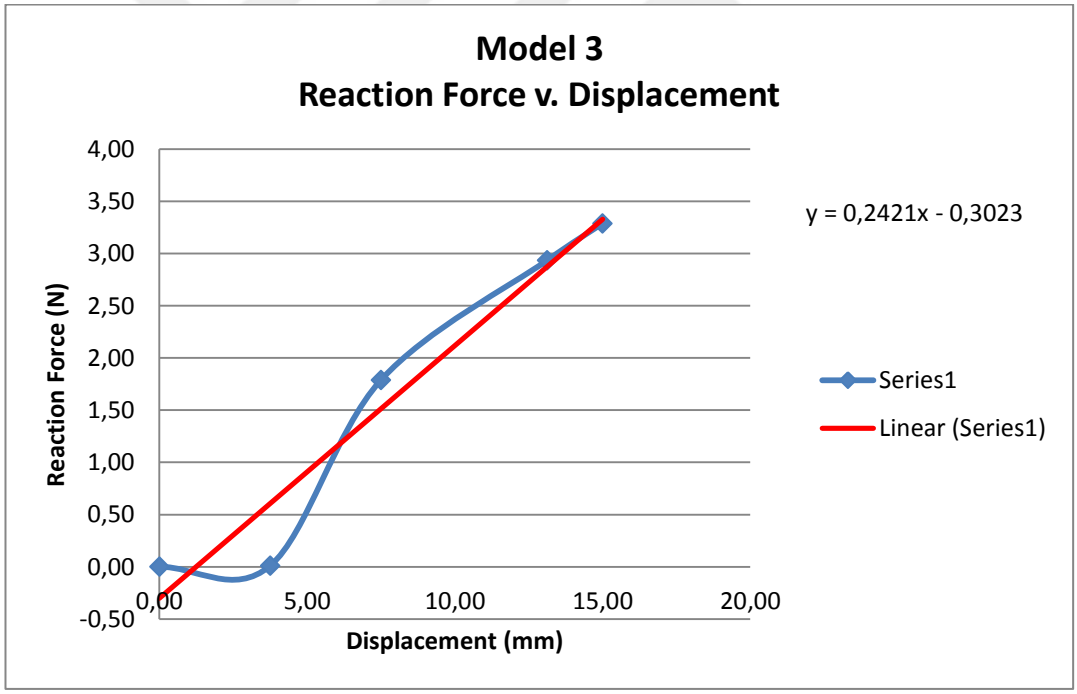

Figure 17: Reaction Force v Displacement graph for Model 3

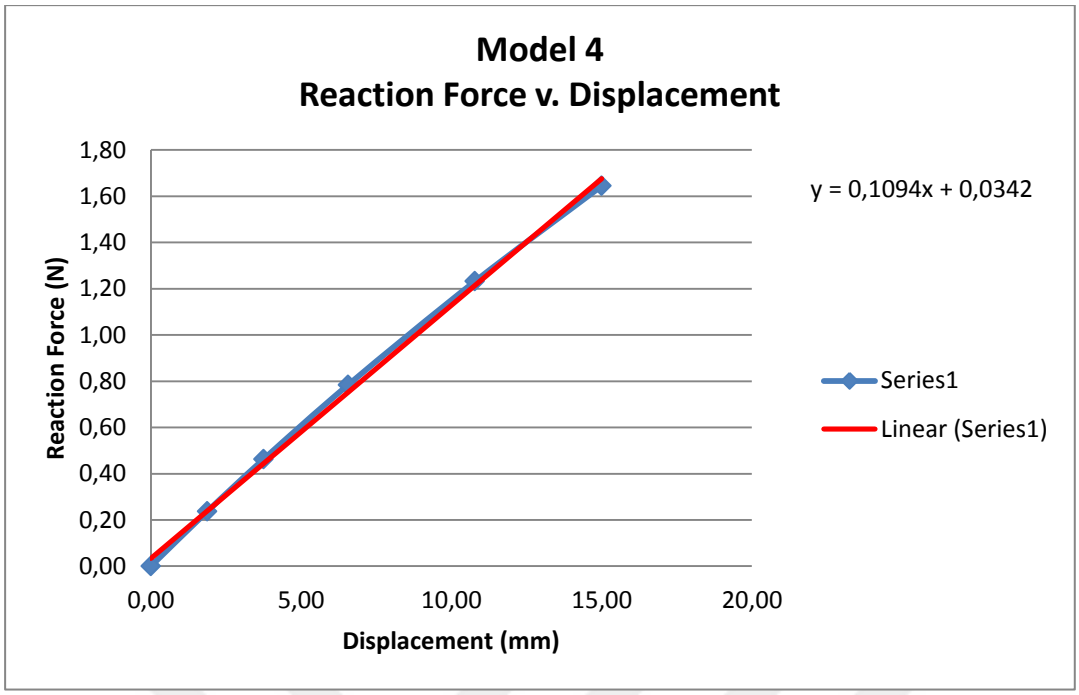

Figure 18: Reaction Force v Displacement graph for Model 4.

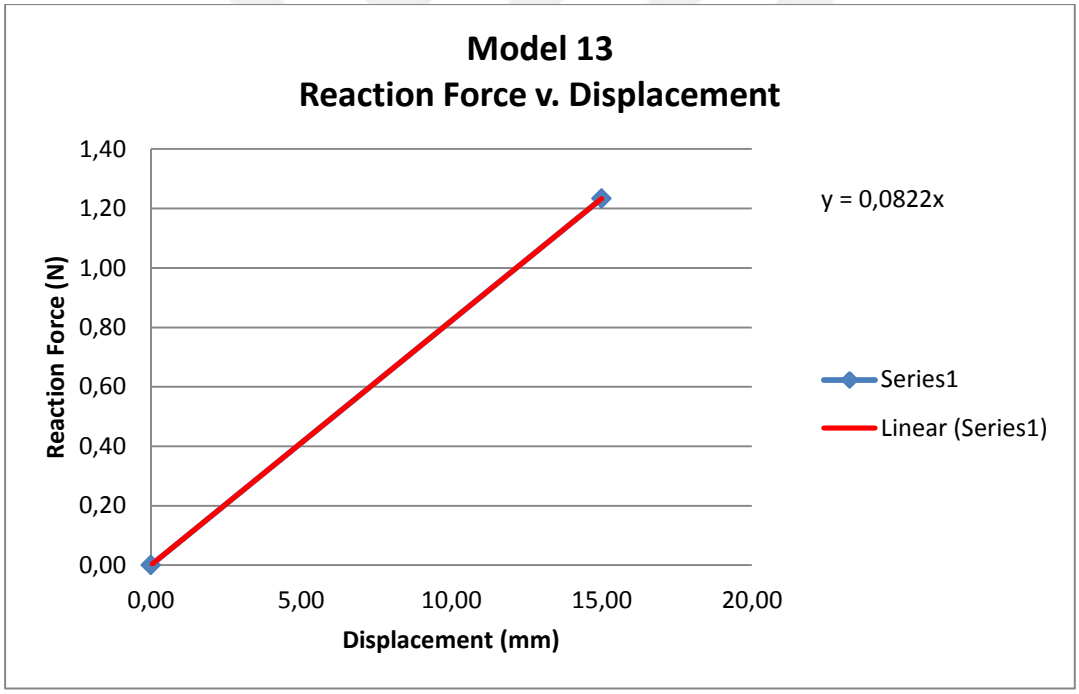

Figure 19: Reaction Force v Displacement graph for Model 13.

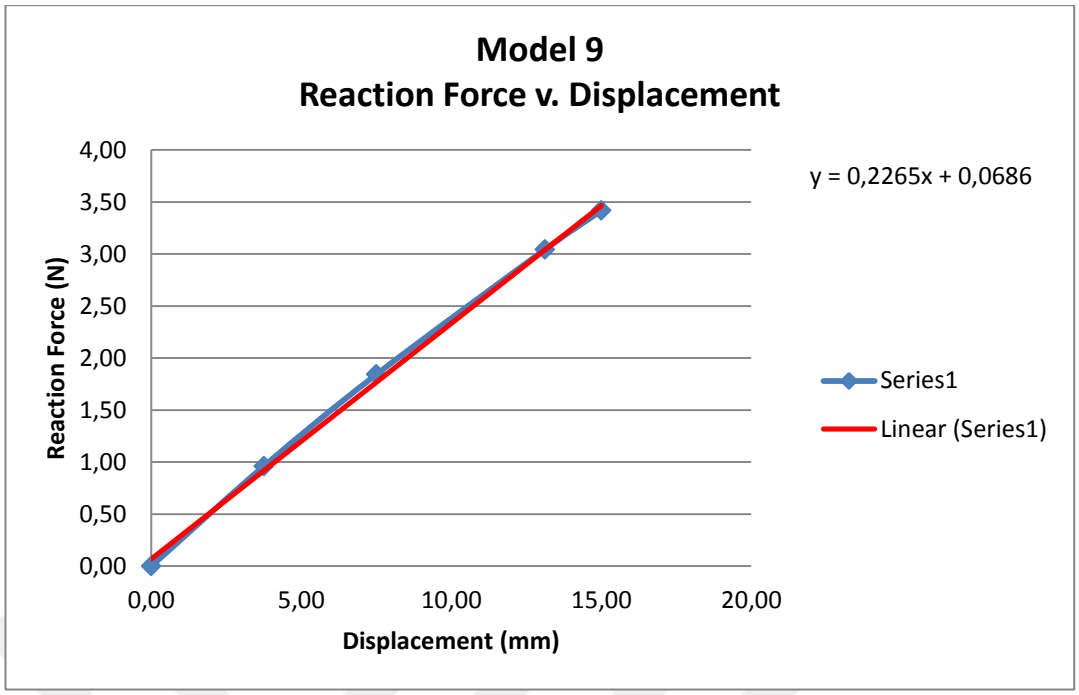

Figure 20: Reaction Force v Displacement graph for Model 9.

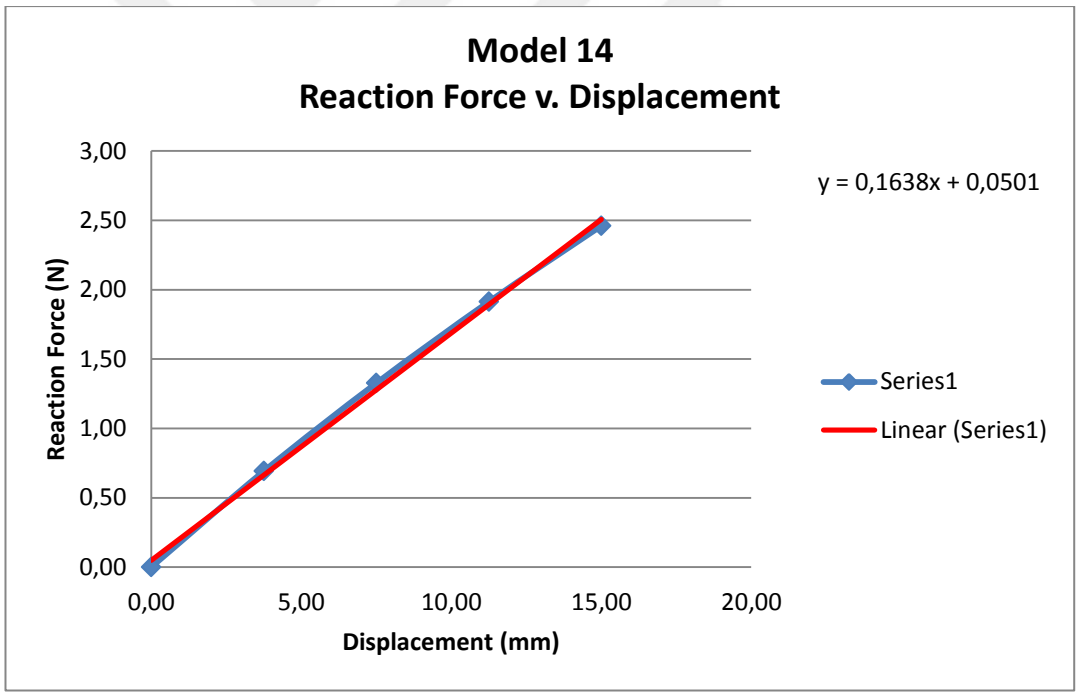

Figure 21: Reaction Force v Displacement graph for Model 14.

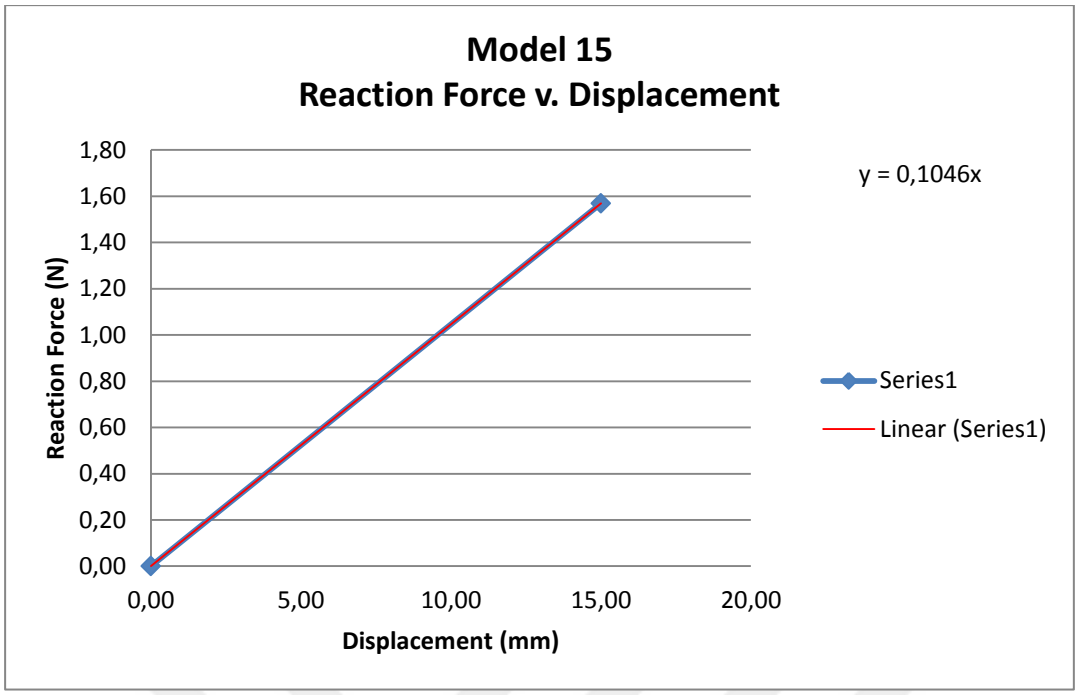

Figure 22: Reaction Force v Displacement graph for Model 15.

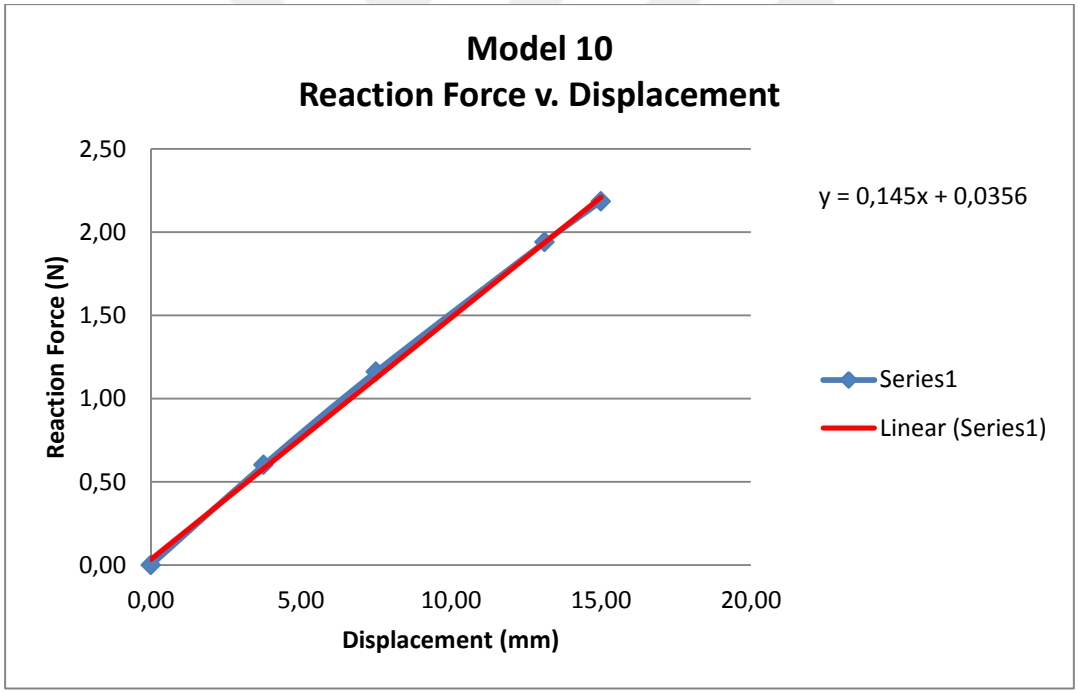

Figure 23: Reaction Force v Displacement graph for Model 10.

To see the effects of the parameters on the equivalent stiffness coefficient the following table can be seen. From this table, the best three models are chosen in order to use in explicit dynamic analyses.

Table 5: All models with their parameters, maximum stress values (for -15 mm displacement) and equivalent stiffness.

CROSS SECTION DIAMETER CONTROL	Cross Section Dia (mm)	Turn Radius (mm)	Number of Turn	Max Stress (MPa)	Equivalent k(N/mm)
Model 3	2,50	2,50	52,00	25,50	0,2421
Model 1	3,75	2,50	52,00	27,87	1,504
Model 2	5,00	2,50	52,00	36,90	-
TURN RADIUS CONTROL					
	Cross Section Dia (mm)	**Turn Radius (mm)**	**Number of Turn**	**Max Stress (MPa)**	**Equivalent k(N/mm)**
Model 3	2,50	2,50	52,00	25,50	0,2421
Model 4	2,50	5,00	52,00	9,30	0,1094
Model 13	2,50	7,50	52,00	8,22	0,0822
NUMBER OF TURN CONTROL					
	Cross Section Dia (mm)	**Turn Radius (mm)**	**Number of Turn**	**Max Stress (MPa)**	**Equivalent k(N/mm)**
Model 4	2,50	5,00	52,00	9,30	0,1094
Model 14	2,50	5,00	40,00	10,88	0,1638
Model 9	2,50	5,00	28,00	11,96	0,2265
NUMBER OF TURN CONTROL (2)					
	Cross Section Dia (mm)	**Turn Radius (mm)**	**Number of Turn**	**Max Stress (MPa)**	**Equivalent k(N/mm)**
Model 13	2,50	7,50	52,00	8,22	0,0822
Model 15	2,50	7,50	40,00	8,97	0,1046
Model 10	2,50	7,50	28,00	6,78	0,145

In the table above, it can be seen that for Model 2 equivalent k cell is empty. Since the yield limit for ABS material is 30.4 MPa, it is obvious that Model 2 fails to have low maximum stress value. The best 3 models are chosen considering their maximum stress values and equivalent stiffness coefficients. The maximum stress value is wanted to be lowest while the equivalent stiffness coefficinet wanted to be the highest.

In the graph above, Maximum Stress v Equivalent Stiffness Coefficient for all models presented in Table 5 can be seen.

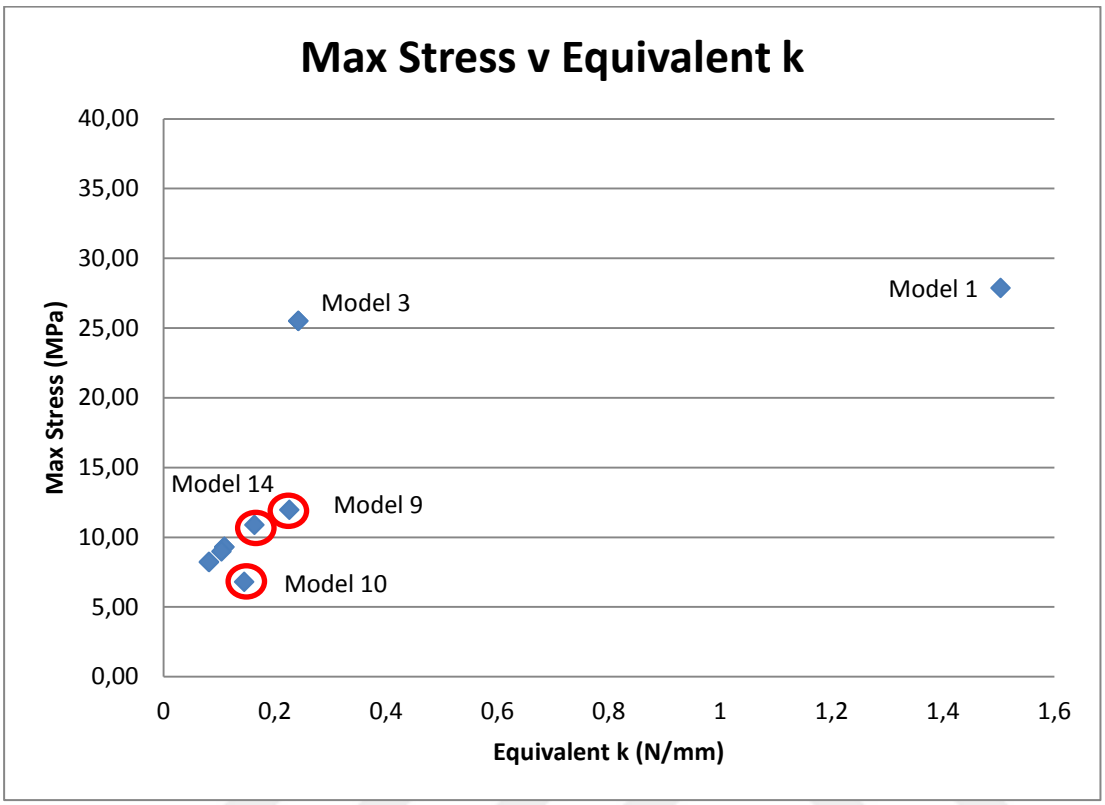

Figure 24: Maximum Stress v Equivalent k graph for models.

In the graph above, it can be seen that Model 1 has the highest stiffness and highest maximum stress value. Having around 30 MPa stress value under -15mm displacement is not allowable. Because it is not hard to tell that it will yield while crashing by the rigid plate. Model 3 has the second highest stiffness among the models, but it still has high maximum stress value, which is really close to the yield limit.

So the next three models with highest stiffness values are chosen to be used in the explicit dynamic analysis as best models. Because, while they have respectively high stiffnesses, they also have low maximum stress values which will allow them to deform freely.

3.4 Material Characterization

In this thesis for the model, material is specified as ABS. As it is mentioned in previous sections, there is a study that investigates the material properties of 3D printed ABS material . (J. Cantrell, S. Rohde, D. Damiani, R. Gurnani, L. DiSandro, J. Anton, A. Young, A. Jerez, D. Steinbach, C. Kroese, P. Ifju, 2017). The stess strain curve of ABS given in this study can be seen below.

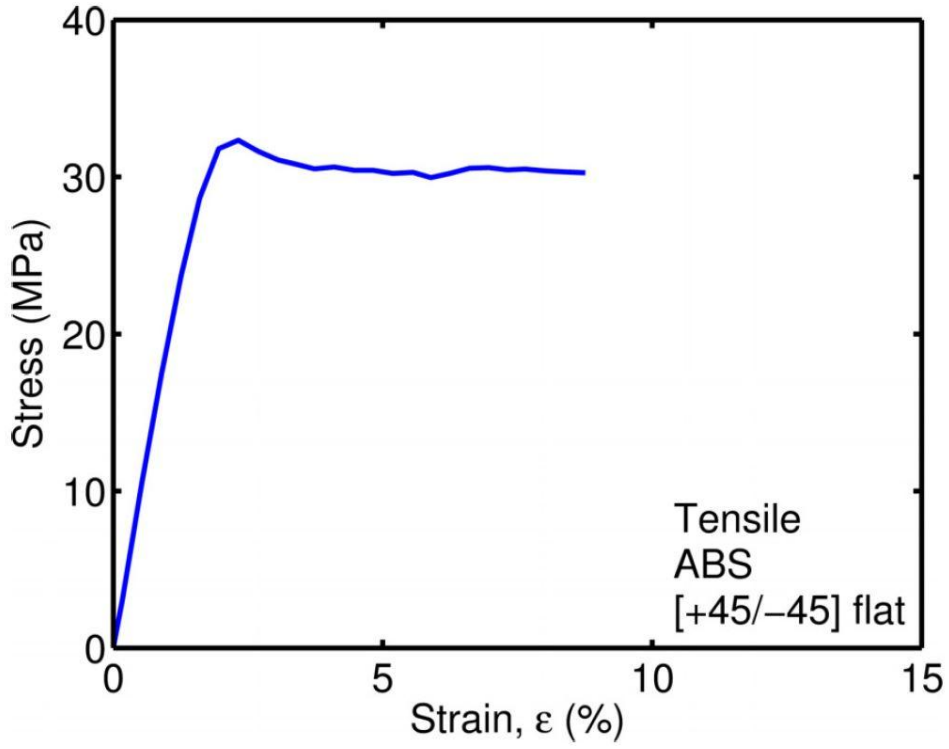

Figure 25: Stress-Strain curve of 3D printed [+45/-45] flat ABS material

The graph above is digitalized in order to acquire plastic stress – plastic strain values to specify the plastic behaviour for the explicit dynamic analyses. The density is specified as 1.04E-9 tonnes/mm^3, yield stress is found as 30.4 MPa, Young's modulus is 2000 MPa, and Poisson's ration is 0.35. The material of the rigid plate is chosen to be steel and its mass is 0.000986125 tonnes, while the material of the sandwich plates are ABS, and 0.001911 tonnes each.

3.5 FEA of The Simplified Sandwich Structure with an Analytical Spring

Since the equivalent stiffness coefficients of the models are calculated, and the best three models among them are chosen, the explicit dynamic analyses are ready to run. In this analysis, the sandwich structure is simplified dramatically. An analytical spring is placed between two sandwich plates. In this way, number of elements and L^e value is decreased considerably. As it is explained in previous chapters, a rigid plate will squeeze this simplified model, the analytical spring will absorb its energy as it is compressed and after the rigid plate stops, the spring will rise it up.

The corresponding simplified sandwich structure consists of 8 unit cells. There are 4 in the first floor, and 4 on top of them in the second floor. This means that, in the simplified model there are 4 parallel springs on the first floor and 4 top of them connected to the first floor in series. From simple calculations, it can be seen that the equivalent stiffness of the sandwich structure is $2k$, where k is the stiffness of an unit cell.

Before presenting the results, the details of the analysis can be seen in the following figure.

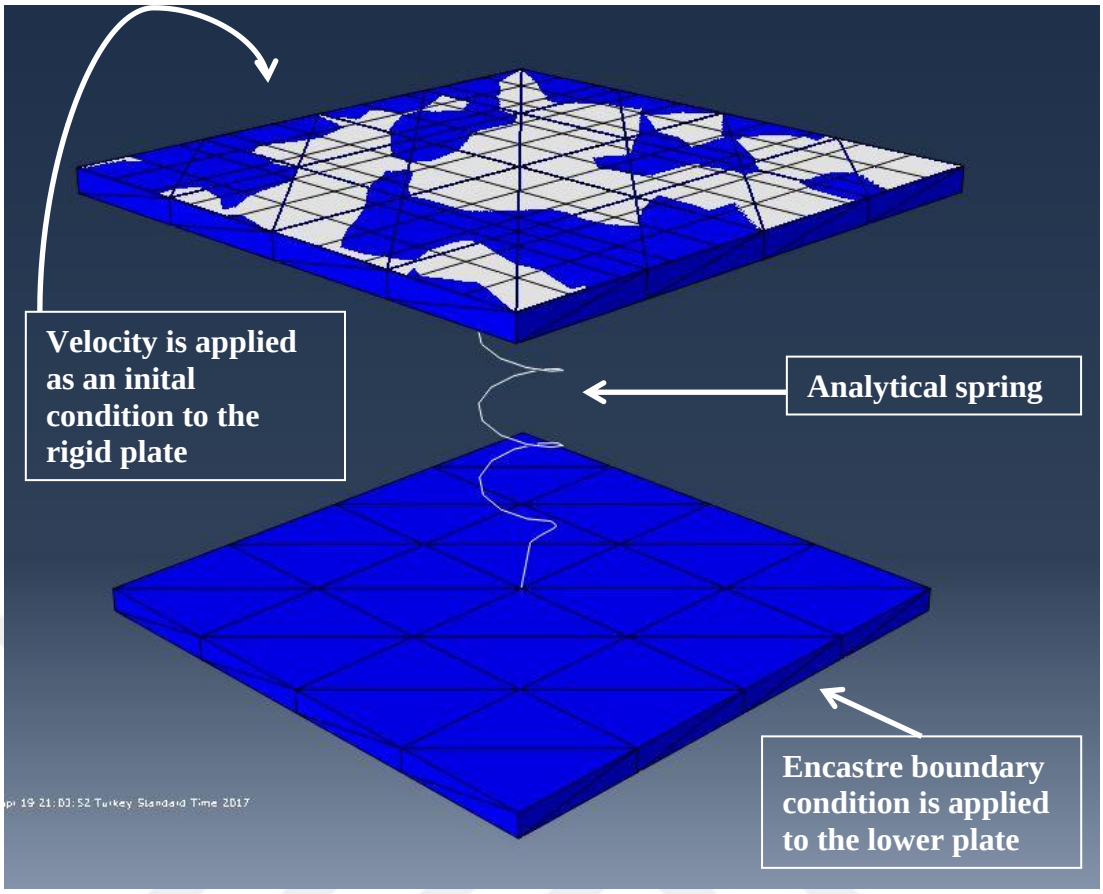

Figure 26: Simplified sandwich structure with an analytical spring.

For the analytical spring, the only parameter specified is the spring constant. As it is mentioned before, the sandwich structures equivalent stiffness is $2k$, where k is the corresponding stiffness coefficient of the unit cell. The spring is connected to the center nodes of both sandwich plates. Then, these center nodes are linked to whole plates surfaces. In addition, the rigid plate is tied to the upper sandwich plate in order to observe the energy absorption better. For the chosen three models, analyses are repeated for 3 different velocities to observe their behaviour with more detail.

For each analysis, velocity v time graphs are plotted, energy absorption and specific energy absorption values are calculated. To calculate energy absorption, firstly the kinetic energy (KE_1) of the rigid plate before collision is calculated. Secondly, the kinetic energy (KE_2) of the plate where it has its maximum velocity in opposite direction is calculated. Lastly, the energy absorption is calculated by subtracting KE_2 value from KE_1. Because KE_2 value is the unabsorved kinetic energy value of the rigid plate and subtracting it from the total value gives the energy absorption value. Later on , by dividing this value to the model's mass, the specific energy absorption is found. The responses of the three models with same initial velocities are plotted in

the same graph to compare them. Both velocity v time and force v displacement graphs can be seen in the next figures for different initial velocities.

In the following figure, the velocity v time data for the models are plotted for 1000 mm/s initial velocity.

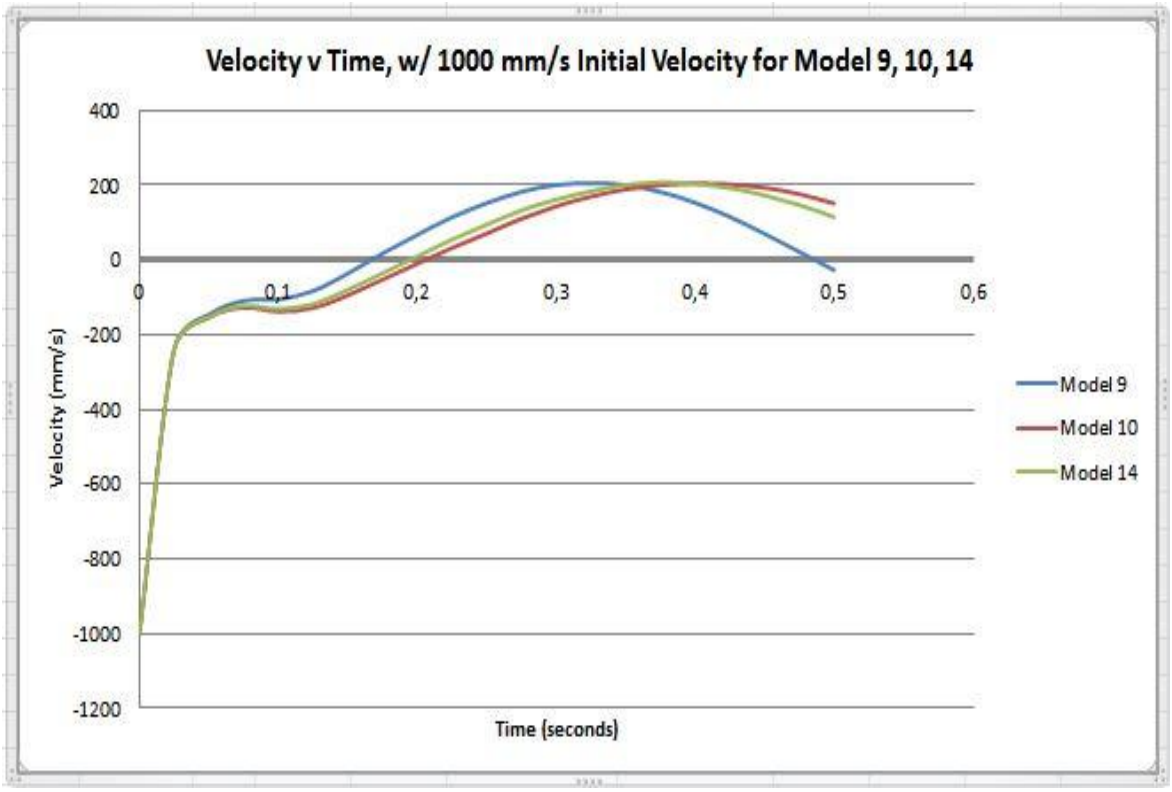

Figure 27: Velocity v Time graph of the models for 1000 mm/s initial velocity for one spring simplification.

In the next figure, the velocity v time data for the models are plotted for 4000 mm/s initial velocity.

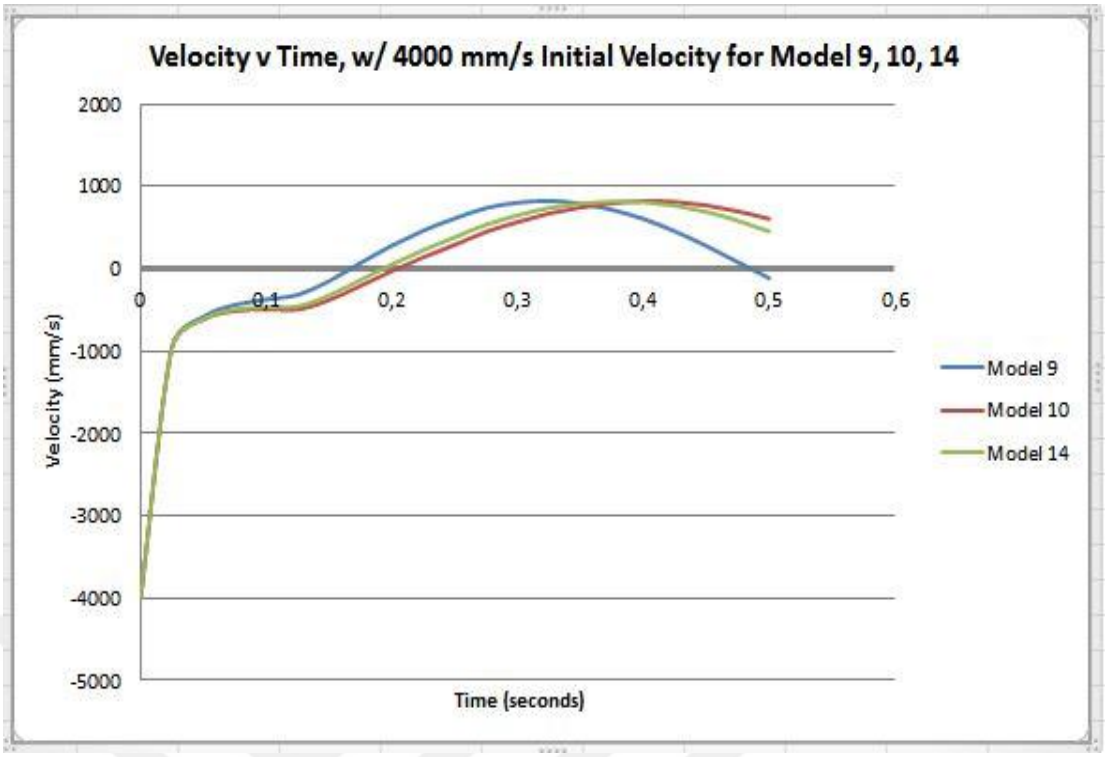

Figure 28: Velocity v Time graph of the models for 4000 mm/s initial velocity for one spring simplification.

Lastly, in the figures below, the velocity v time and force v displacement data for the models are plotted for 8000 mm/s initial velocity.

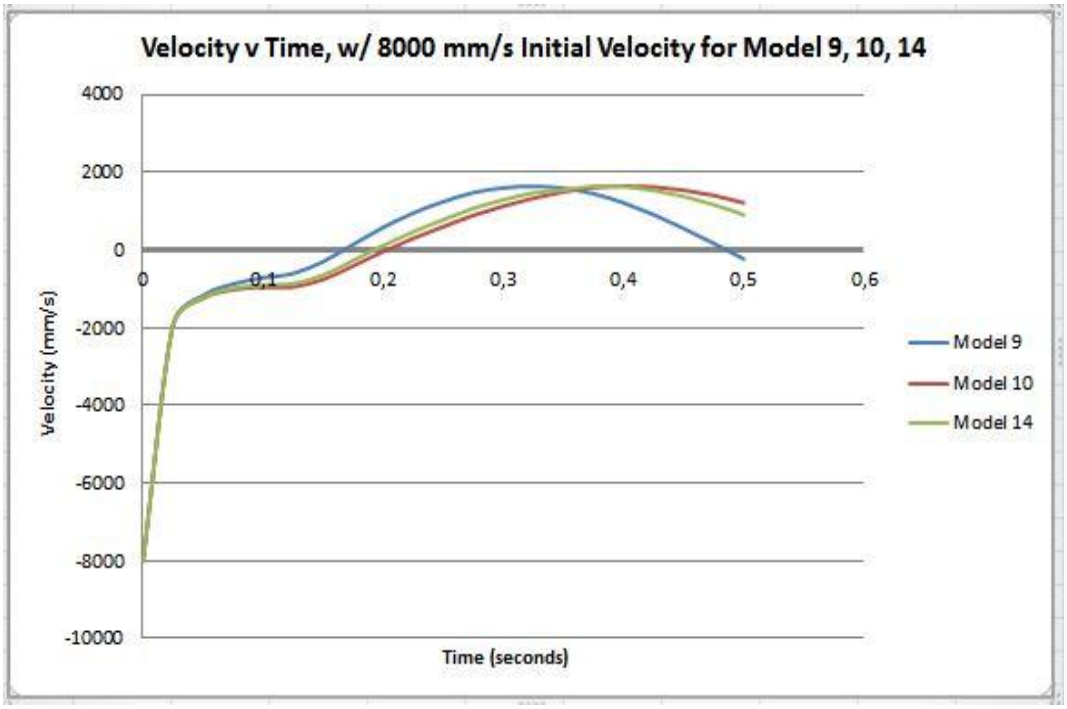

Figure 29: Velocity v Time graph of the models for 8000 mm/s initial velocity for one spring simplification.

For the velocity v time graphs, it can be easily seen that Model 10 and Model 14 have very similar reactions to the rigid plate, no matter what the initial velocity is. The fastest reaction to the rigid plate is given by the Model 9 among those three models. From the velocity v time graphs, it is obvious that Model 9 stops the rigid plate first among these models. It means that, Model 9 absorbs the kinetic energy of the rigid plate fastest. Both Model 10 and Model 14 absorbs the all kinetic energy of the rigid plate around 0.2 seconds. For Model 9 this time is around 0.16 seconds. And also from these velocity v time graphs, it can be easily seen that Model 9's response time is much lower, because when the Model 9 data is checked it can be observed that the rigid plate's velocity becomes zero two times. Which means, for Model 9, after expanding and rising the plate up, it reaches to its maximum height and stops. For all models, the velocity decreases dramatically in the first 0.05 seconds, and this part of the graph can defined as linear. Also the responses of the models are so close that they look overlapped. Later on, after this dramatic decrease all models have a small plateu for around 0.05 seconds, which is much lesser for Model 9. The difference between those plateu fields have a vital role for the reaction time of the Models. After this steady-like period, until the velocity reaches zero, the velocity decreases slowly.

As it is mentioned previously, the energy absorptions of the models are calculated from velocity v time graphs. The method is mentioned previously, which is subtracting the residual kinetic energy of the rigid plate from the inital and total kinetic energy. It is obvious that this difference between those values gives the energy absorption value. And by dividing it by the models' masses the specific energy absorption of each model can be calculated for different velocities.

In the following table the energy absorption data of the models can be seen.

Table 6: Energy absorption table of the sandwich structure with one spring simplification.

ENERGY ABSORPTION TABLE OF THE SANDWICH STRUCTURE W/ ONE SPRING SIMPLIFICATION					
Model 9	V1 (m/s)	Vmax (m/s)	Energy Absorbed (J)	Specific Energy (J/kg)	Mass (kg)
1000 mm/s	1	0,204	1,96	0,479	4,1
4000 mm/s	4	0,822	31,41	7,66	4,1
8000 mm/s	8	1,634	125,72	30,664	4,1
Model 10	V1 (m/s)	Vmax (m/s)	Energy Absorbed (J)	Specific Energy (J/kg)	Mass (kg)
1000 mm/s	1	0,204	2,036	0,479	4,25
4000 mm/s	4	0,820	32,57	7,663	4,25
8000 mm/s	8	1,643	130,2	30,649	4,25
Model 14	V1 (m/s)	Vmax (m/s)	Energy Absorbed (J)	Specific Energy (J/kg)	Mass (kg)
1000 mm/s	1	0,206	2,024	0,478	4,23
4000 mm/s	4	0,815	32,43	7,667	4,23
8000 mm/s	8	1,640	129,67	30,654	4,23

In the table above, the energy absorption and specific energy absorption values of the each model for different initial velocities for one spring simplification are presented. When the energy absorption values are investigated for each model, it can be seen that results are very close to each other. But without any exceptions, Model 9's total energy absorption values for each initial velocities are the lowest. Even there are differences between energy absorption capabilites of the models, the differences are negligible. Also again, the differences between specific energy capabilites of the models are not that large. But as it is mentioned previously, like in the velocity v time graphs, Model 10's and Model 14's results are almost identical.

3.6 FEA of The Simplified Sandwich Structure with 8 Analytical Springs

Since the actual sandwich structure has 8 unit cells, simplifying it with 8 analytical springs can give more realistic results. Also the equivalent stiffness values are calculated for unit cells, and each of them acts like an individual spring in the actual model. Different from the previous chapter, the equivalent value of 8 springs are not calculated and the analyses are made with 8 identical springs. So in this chapter, the responses of the simplified sandwich structure with 8 analytical springs are presented. In the following figure, the FEA model of this simplified model can be seen. As it can be seen, there are 4 analytical springs in the first floor and 4 on top of them. Each spring shares a node with the spring which is connected in series with it.

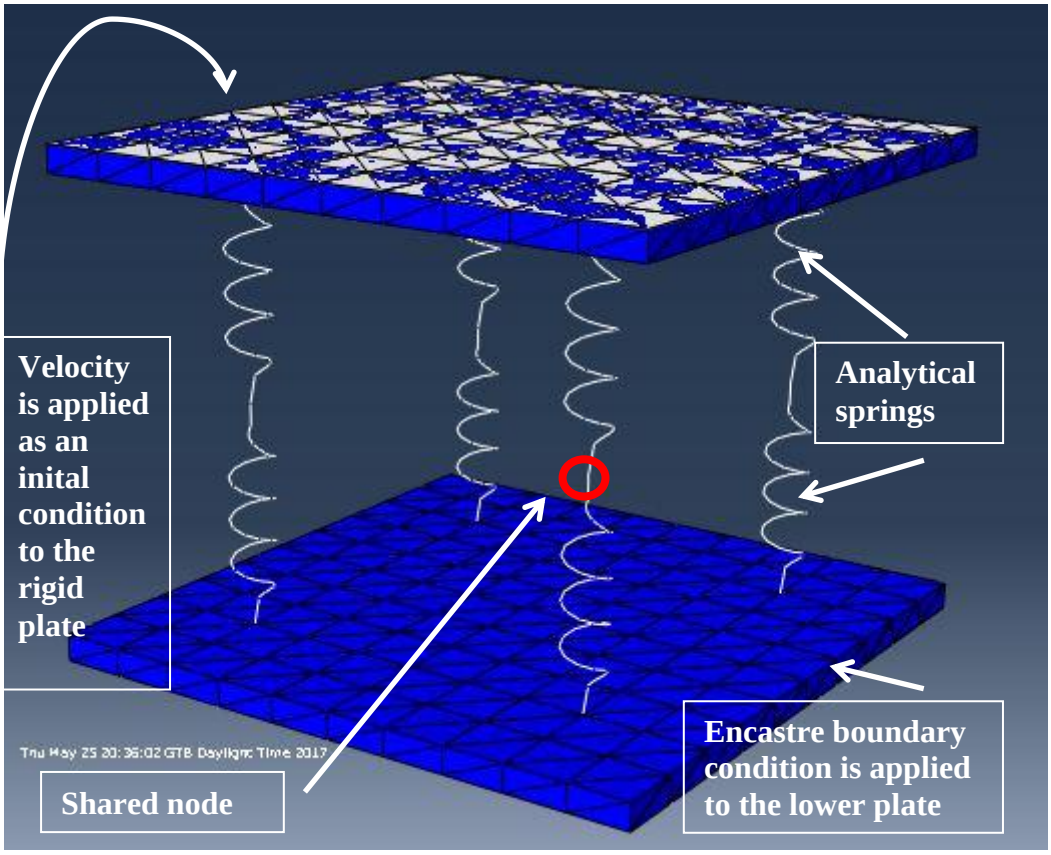

Figure 30: FEA model of the simplified sandwich structure with 8 analytical springs.

In this simplified model the initial conditions, boundary conditions and loads are all identical with the previous simplified model which is simplified with an only one analytical spring.

In the following figure, the velocity v time data for the models are plotted for 1000 mm/s initial velocity.

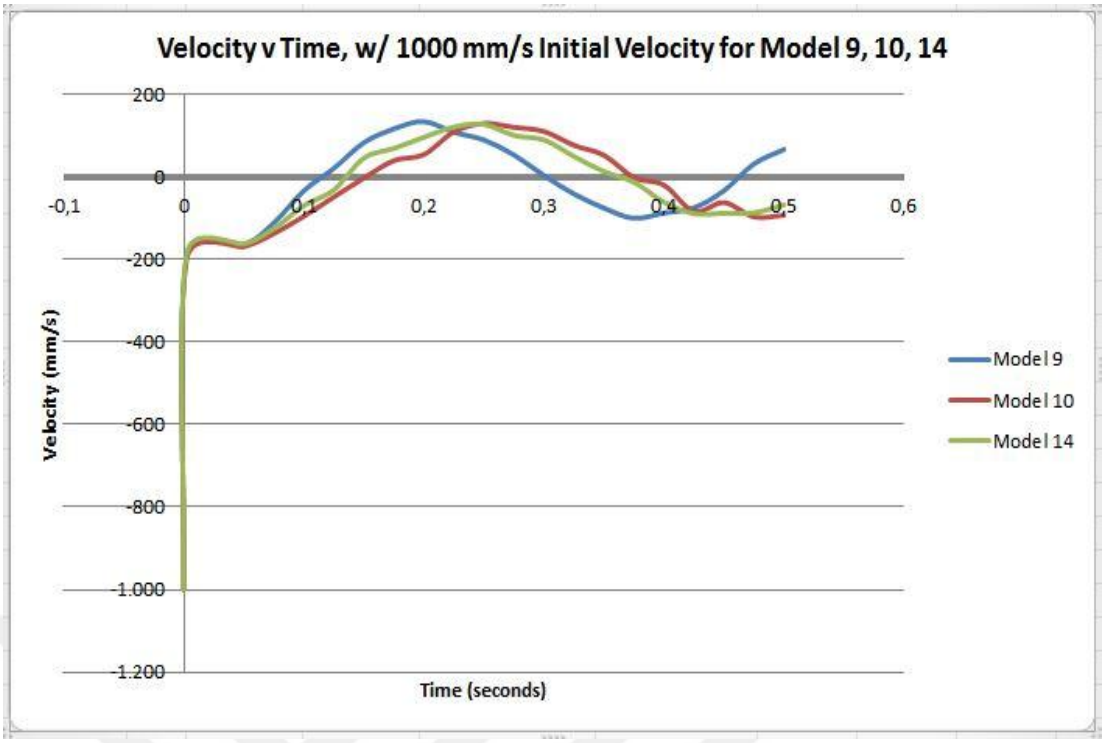

Figure 31: Velocity v Time graph of the models for 1000 mm/s initial velocity for 8 spring simplification.

In the next figure, the velocity v time data for the models are plotted for 4000 mm/s inital velocity.

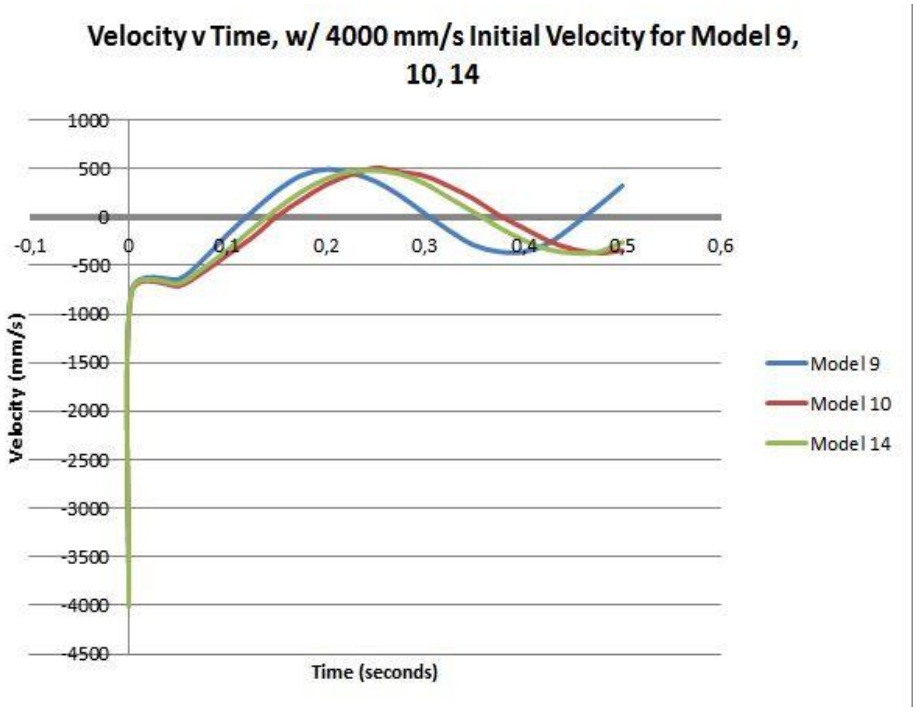

Figure 32: Velocity v Time graph of the models for 4000 mm/s initial velocity for 8 spring simplification.

In the following figure, the velocity v time data for the models are plotted for 8000 mm/s.

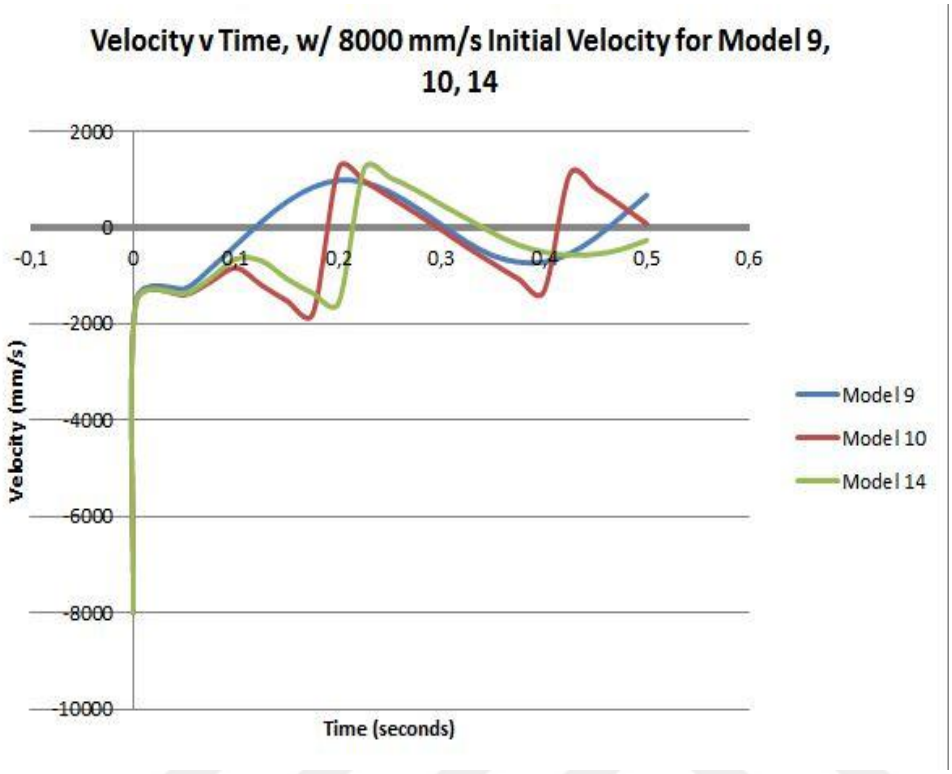

Figure 33: Velocity v Time graph of the models for 8000 mm/s initial velocity for 8 spring simplification.

For the velocity v time graphs for 1000 mm/s and 4000 mm/s initial velocities, again the fastest response is given by Model 9. It can be seen that, Model 9 stops the rigid plate at around 0,1 seconds. For one spring simplifaction, this period was around 0,15 seconds. And again, Model 10 and Model 14 responds to the plate slower than Model 9. They stop the rigid plate around 0.15 seconds, which is faster than one spring simplification results. Generally, it can be said that with 8 springs, the models' responses are much faster. Differently from the one spring simplification results, the responses are much more similar for all 3 models for 8 spring simplification. Model 10 and Model 14 are almost identical again, but they are much more closer to Model 9 according to these results. For 8000 mm/s results, it can be easily seen that, there are some jumps in Model 10 and Model 14 lines. Differently from all other results presented previously, before stopping the rigid plate, the rigid plate's velocity increases. It is not an expected result. Around 0,1 seconds, while Model 9 stops the rigid plate, for Model 10 and Model 14 velocity increases. One reason causing this can be that Model 10 and Model 14 have lower stiffness constants than Model 9.

Since this unexpected results occur with highest initial velocity, it can be acceptable. Even Model 10 and Model 14 stops the rigid plate much later than Model 9, their energy absorption values are close to each other. Because it can be seen that the difference between their maximum velocity values in opposite direction is not that large.

In the following table, the energy absorption data for 8 spring simplifaction can be seen.

Table 7: Energy absorption table of the sandwich structure with eight spring simplification**.**

ENERGY ABSORPTION TABLE OF THE SANDWICH STRUCTURE W/ EIGHT SPRING SIMPLIFICATION					
Model 9	V1 (m/s)	Vmax (m/s)	Energy Absorbed (J)	Specific Energy (J/kg)	Mass (kg)
1000 mm/s	1	0,133	2,013	0,491	4,1
4000 mm/s	4	0,488	32,310	7,880	4,1
8000 mm/s	8	0,977	129,242	31,522	4,1
Model 10	V1 (m/s)	Vmax (m/s)	Energy Absorbed (J)	Specific Energy (J/kg)	Mass (kg)
1000 mm/s	1	0,129	2,0893	0,491	4,25
4000 mm/s	4	0,502	33,462	7,873	4,25
8000 mm/s	8	1,229	132,787	31,244	4,25
Model 14	V1 (m/s)	Vmax (m/s)	Energy Absorbed (J)	Specific Energy (J/kg)	Mass (kg)
1000 mm/s	1	0,127	2,080	0,491	4,23
4000 mm/s	4	0,477	33,357	7,885	4,23
8000 mm/s	8	1,221	132,206	31,254	4,23

In the table above, the energy absorption and specific energy absorption values of the each model for different initial velocities for 8 spring simplification are presented. When the energy absorption values are investigated for each model, it can be seen that results are very close to each other, like one spring simplification. Even there are differences between energy absorption capabilites of the models, the differences are negligible. Also again, the differences between specific energy capabilites of the models are not that large. But as it is mentioned previously, like in the velocity v

time graphs, Model 10's and Model 14's results are almost identical. The only difference here is, the overall similarity of all three models are much more.

3.7 FEA of The Actual Sandwich Structure

As it is mentioned previously in this chapter, the explicit dynamic analysis of the sandwich structure takes a very long time. The reasons of this was explained in Explicit Dynamics chapter and Stable Time Increment chapter. So, as a solution the model was simplified with a analytical springs and then analyzed. But to verify these simplified results, the same analysis is run for the actual sandwich structure for a shorter period of time. This specified period of time is enough to calculate the specific energy absorption. It means that, the rigid plate stops in this time period. Since it is not necessary to know what happens after the rigid plate has its maximum velocity in opposite direction. Because to calculate the energy absorption and specific energy absorption, the data will be enough. Also the velocity time graphs of the rigid plates for actual and simplified models are compared for the corresponding period of time.

For the actual sandwich structure analysis, Model 10 is chosen and the initial velocity of the rigid plate is specified as 1000 mm/s.

In this analysis, the model is meshed with tetrahedral elements of type C3D4 since Abaqus explicit only lets to use this type of tetrahedral elements. In this analysis, the total number of nodes is 561670, number of elements is 1796541. Number of linear tetrahedral elements are 1796441 and remaining 100 elements are linear quadrilateral elements of type R3D4, which are used to mesh the rigid plate.

Similarly to the simplified models, the lower plate is specified as encastre, the initial velocity is applied to the rigid plate, rigid plate and the top plate is tied. The meshed model can be seen in the following figure.

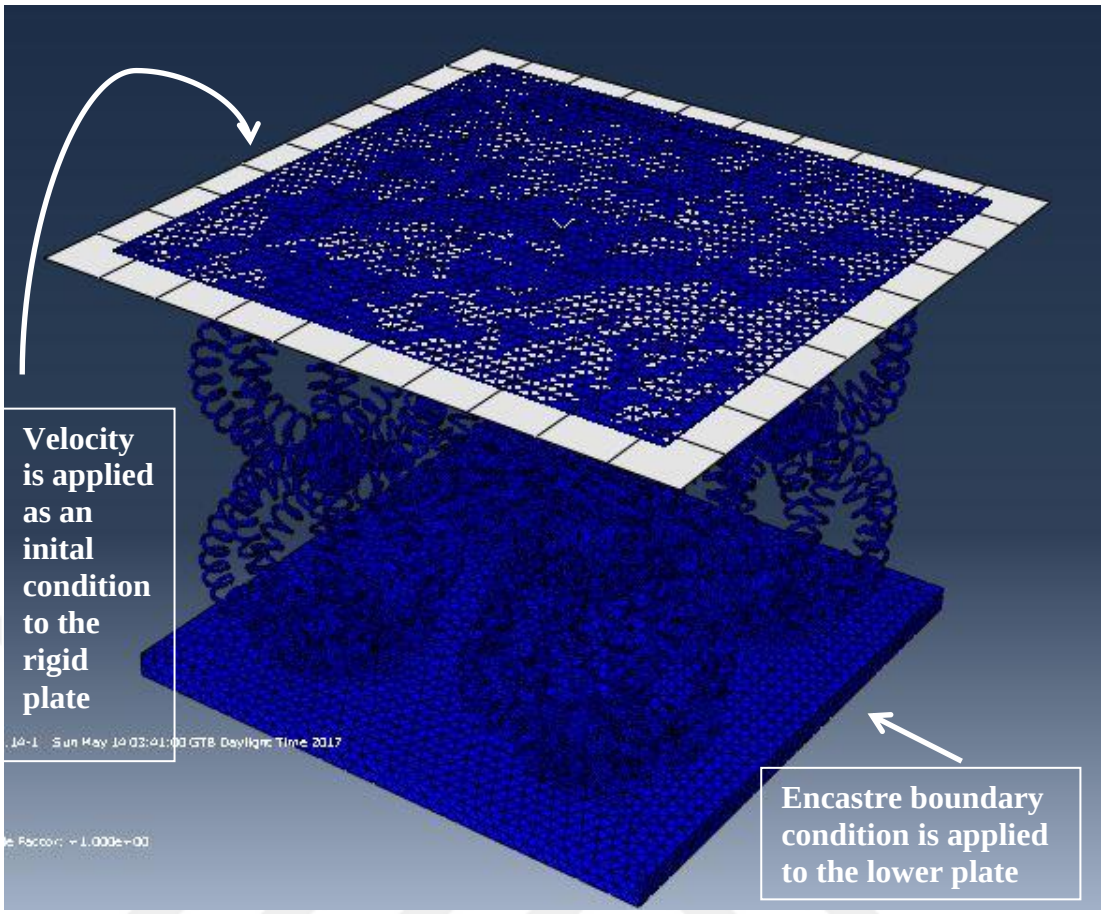

Figure 34: FEA model of the actual model.

The velocity v time graph of this analysis compared with simplified models can be seen in the following figure.

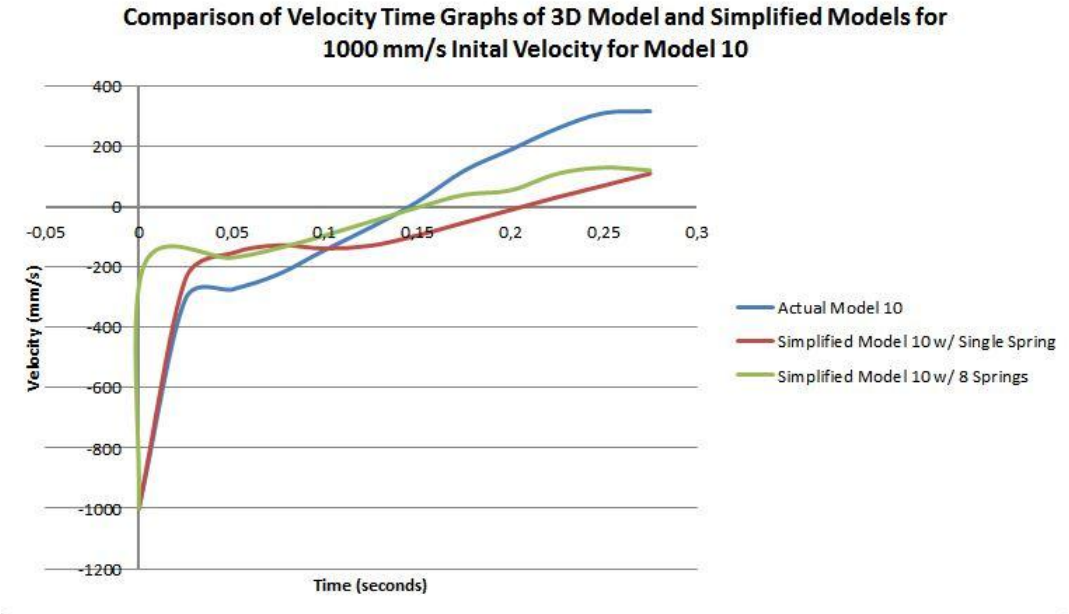

Figure 35: Comparison of Velocity v Time graphs of actual and simplified models for 1000 mm/s initial velocity for Model 10

From the graph in previous page, it can be seen that the rigid plate stops around 0,1 seconds for all three models. Since the simplified models decrease the analysis time dramatically, it is possible to use simplified models to find this result. It can save a lot of time and money. So it is useful to have this results being consistent. The another important variable is the maximum velocity that the rigid plate gains in opposite direction. This variable is used to calculate the energy absorption value and it can be easily seen that there is a difference between actual and simplified models.The difference caused by this will be discussed in next chapter, but if the data is compared it can be seen that the difference is not large.

To see the energy absorption data of the actual model the following table can seen.

Table 8: Energy absorption table of the actual model 10.

ENERGY ABSORPTION TABLE OF THE ACTUAL MODEL 10				
Model 10	V1	Vmax	Energy Absorbed	Specific Energy
1000 mm/s	1	0,316377	1,912	0,449

4. DISCUSSION AND CONCLUSION

In this chapter a comparison of all of the models are presented, and discussed. The advantages and disadvantages of the two kind of simplfications will be concluded.

In the following table, the comparison of all analyses made can be seen.

From the following table, it can be seen that the energy absorption values for one spring simplification, eight spring simplification and for actual model are consistent. In figure 34, it is seen that the maximum velocity of the rigid plate in opposite direction was different in actual model. But from the following table, it is seen that the difference is negligible, since the energy absorption and specific energy absorption data are similar.

Also it can be seen that, the model, which is simplified by 8 analytical springs, stops the rigid plate at the same time with the actual model. Since analyzing the actual 3D model takes very long time, one can use this simplification method to estimate the rigid plate's stopping time. This method will save a lot of time, because the actual 3D model has very small characteristic element length, which leads to having very small stable time increment. Since in the simplified model, whole design is simplified to analytical springs, analysis time is decreased dramatically.

In the figure 34, it can be seen that the velocity decrease is much larger for 8 spring model than other two models at the very beinning. While the 1 spring model estimates the behaviour of the 3D model better at the beginning, the 8 spring model estimates the exact time of the rigid plate's stopping time.

Lastly, it can be seen that both simplified models' have similar results in means of the rigid plate's maximum velocity at opposite direction. But both of them are not similar to the actual 3D model's results.

At first look, it can be said that the difference is large. But, when the results in the following table is examined, the results are acceptable. Since the energy absorption of the models are calculated by referencing the rigid plate's kinetic energy, the most important data from all of the presented Velocity v Time graphs are the rigid plate's initial velocity and the rigid plate's maximum velocity in the opposite direction. Because the energy absorption of the model is calculated by subtracting the kinetic energy, where the rigid plate has its maximum velocity in opposite direction, from the initial kinetic energy.

In the following table, Table 9 in the next page, the energy absorption data can be found. As it is mentioned previously the results are very close to each other. Also in the same table, specific energy absorption data of the 3D actual model for model 10, and the both simplified analyses for all three models can be seen. And again, it is possible to see that the results are again very close, as it is expected.

Table 9: Energy absorption of the sandwich structures for model 9, 10, 14.

ENERGY ABSORPTION OF THE SANDWICH STRUCTURES FOR MODEL 9, 10, 14					
	Initial Velocity (mm/s)	**Mass (kg)**	**Energy Absorption (1 Spring) (Joule)**	**Energy Absorption (8 Springs) (Joule)**	**Energy Absorption (Actual) (Joule)**
Model 9 (4x2)	1000	4,10	1,964125892	2,013191848	-
	4000	4,10	31,41152954	32,31010264	-
	8000	4,10	125,7251162	129,2420657	-
Model 10 (4x2)	1000	4,25	2,036118062	2,089367622	1,912299387
	4000	4,25	32,57102802	33,46253543	-
	8000	4,25	130,2601091	132,7878575	-
Model 14 (4x2)	1000	4,23	2,024548528	2,080745194	-
	4000	4,23	32,43492969	33,35742739	-
	8000	4,23	129,670386	132,2068196	-
	Initial Velocity (mm/s)	**Mass (kg)**	**Specific Energy Absorption (1 Spring) (Joule/kg)**	**Specific Energy Absorption (8 Springs) (Joule/kg)**	**Specific Energy Absorption (Actual) (Joule/kg)**
Model 9 (4x2)	1000	4,10	0,47929766	0,491271026	-
	4000	4,10	7,665227904	7,884503047	-
	8000	4,10	30,6801892	31,5384161	-
Model 10 (4x2)	1000	4,25	0,478687143	0,491206004	0,449577629
	4000	4,25	7,657381286	7,866972833	-
	8000	4,25	30,62388209	31,2181505	-
Model 14 (4x2)	1000	4,23	0,4788786	0,492171135	-
	4000	4,23	7,672028366	7,890232278	-
	8000	4,23	30,67171377	31,27167163	-

REFERENCES

K. Li, X. –L. Gao, G. Subhash (2005) *Effects of cell shape and strut cross-sectional area variations on the elastic properties of three-dimensional open-cell foams*, Journal of The Mechanics and Physics of Solids 54 (2006) 783-806

Gebhardt A. (2011). *Understanding Additive Manufacturing, Rapid Prototyping, Rapid Tooling, Rapid Manufacturing,* Munich – Hanser Publishers

Cantrell J. et al. (2017). *Experimental Characterization of the Mechanical Properties of 3D-Printed ABS and Polycarbonate Parts,* In: Yoshida S., Lamberti L., Sciammarella C. (eds) Advancement of Optical Methods in Experimental Mechanics, Volume 3, Conference Proceedings of the Society for Experimental Mechanics Series. Springer, Cham

T. Tancogne-Dejeab et al. (2016). *Additively-manufactured mettalic micro-lattice materials for high specific energy absorption under static and dynamic loading,* Acta Materialia 116 (2016) 14-28

C. Yan et al. (2014). *Advanced lightweight 316L stainless steel cellular lattice structures fabricated via selective laser melting,* Materials and Design 55 (2014) 533-541

Bauer. J, Schroer S., Schwaiger R., Kraft O. (2016). *Approaching theoretical strength in glassy carbon nanolattices*. Nature Materials (2016) DOI: 10.1038/NMAT 4561.

Klahn, C., Leutenecker, B., & Meboldt, M. (2014). *Design for Additive Manufacturing – Supporting the Substitution of Components in Series Products*. 24th CIRP Design Conference (pp. 138-143). Zurich,: Elsevier B.V.

G. Zhang, B. Wang, Li Ma, L. Wu, S. Pan, J. Yang (2013). *Energy absorption and low velocity impact response of polyurethane foam filled pyramidal lattice core sandwich panels,* Composite Structures 108 (2013) 304-310

S. Soe et. al (2013). *Evaluating Innovative CAD Techniques in the Creation of Conformal Cellular Structures*, Sustainable Design and Manufacturing DOI 10.1007/978-3-319-32098-4_33

C. Yan, L. Hao, A. Hussein, S. L. Bubb, P. Young, D. Raymont (2014). *Evaluation of light-weight AlSi10Mg periodic cellular lattice structures fabricated via direct metal laser sintering*, Journal of Materials Processing Technology 214 (2014) 856-864

N. Michailidis, F. S. (2010). *FEM modeling of the response of porous Al in compression*. Computational Materials Science, 282-286.

X. An, H. Fan (2016). *Hybrid design and energy absorption of luffa-sponge-like hierarchical cellular structures*. Materials and Design 106 (2016) 247-257.

Gibson, I., Rosen, D., & Stucker, B. (2010). *Additive Manufacturing Technologies: Rapid Prototyping to Direct Digital Manifacturing.* New York: Springer.

Lorna J. Gibson, M. F. Ashby (1997). *Cellular Solids, Structure and poperties.* Cambridge Solid State Science Series

Li Yang Ola A Harrysson Harvey A West II Denis R. Cormier Chun Parl Kara Peters (2015). *Low energy drop weght performance of cellular sandwich panels.* Rapid Prototyping Journal, Vol 21 Iss 4 pp. 433-442

F.Ashby, M., J.Gibson, L., Evans, A., Fleck, N., Hutchinson, J., & Wadley, H. (2000). *Metal Foams: A Design Guid.* Butterworth-Heineman.

Nguyen, V.-D., & Noels, L. (2014). *Computational homogenization of cellular materials*. International Journal of Solids and Structures, 2183-2203.

S.K. Nammi, P. M. (2010). *Finite element analysis of closed-cell aluminium foam under quasi-static loading*. Material and Design, 712-722.

J. Brennan-Craddock, D. Brackett, R. Wildman, R Hague (2012). *The design of impact absorbing structures for additive manufacture*. Journal of Physics: Conferece Series 382 (2012) 012042.

R. D. Cook et. al (2002). *Concepts and Applications of finite Element Analysis, 4th Edition*. Wiley, John Wiley & Sons, New York

CURRICULUM VITAE

Name Surname **: Aren Sercan Boyacı**

Place and Date of Birth **: Istanbul / 16.03.1992**

E-Mail **: arenboyaci@gmail.com**

EDUCATION **:**

- **B.Sc.** **:** 2015, Yeditepe University, Faculty of Engineering and Architecture, Mechanical Engineering Department
- **B.Sc.** **:** Erasmus Fall 2014, Windesheim Universiy of Applied Sciences, Engineering Faculty, Mechanical Engineering Department
- **Minor B.Sc.** **:** 2015, Yeditepe University, Faculty of Economics and Administrative Sciences, Business Administration Department
- **M.Sc.** **:** 2017, Istanbul Technical University, Mechanical Engineering Department, Solid Mechanics Programme

PROFESSIONAL EXPERIENCES:

- Research and Development Engineer at Karyer Heat Exchangers (July 2014 – September 2014)
- Student Worker at MechDes Engineering (February 2014 – June 2014)
- Intern at Karyer Heat Exchangers (July 2013 – August 2013)
- Intern at Alarko – Carrier (August 2012)

LANGUAGES:

- English (Full professional proficieny – TOEFL: 95)
- Turkish (Native)
- Armenian (Native)
- Dutch (Elementary)

COMPUTER SKILLS:

Solidworks, Abaqus, MATLAB, MS Office, Altair Hyperworks (Hypermesh), C Language

PROJECTS:

- American Society of Mechanical Engineers (ASME), Student Professional Development Conference (SPDC) 2015, Robots for Relief design competition 4th place
- Bachelor Thesis: A Resilient Platform for Ipad Weight Scale
- Erasmus Term Project: A Tool Concept for Dismantling an Oil Platform Placed in Sea
- Master Thesis: A Novel Spring-Like Cellular Structure Design for Energy Absorbing Applications